JOURNAL OF GEOPHYSICAL RESEARCH, VOL. 102, NO. D23, PAGES 28,447–28,468, DECEMBER 20, 1997

Implications of large scale shifts in tropospheric NO_x levels in the remote tropical Pacific

J. H. Crawford,[1,4] D. D. Davis,[1] G. Chen,[1] J. Bradshaw,[1] S. Sandholm,[1] Y. Kondo,[2] J. Merrill,[3] S. Liu,[1] E. Browell,[4] G. Gregory,[4] B. Anderson,[4] G. Sachse,[4] J. Barrick,[4] D. Blake,[5] R. Talbot,[6] and R. Pueschel[7]

Abstract. A major observation recorded during NASA's western Pacific Exploratory Mission (PEM-West B) was the large shift in tropical NO levels as a function of geographical location. High-altitude NO levels exceeding 100 pptv were observed during portions of tropical flights 5-8, while values almost never exceeded 20 pptv during tropical flights 9 and 10. The geographical regions encompassing these two flight groupings are here labeled "high" and "low" NO_x regimes. A comparison of these two regimes, based on back trajectories and chemical tracers, suggests that air parcels in both were strongly influenced by deep convection. The low NO_x regime appears to have been predominantly impacted by marine convection, whereas the high NO_x regime shows evidence of having been more influenced by deep convection over a continental land mass. DMSP satellite observations point strongly toward lightning as the major source of NO_x in the latter regime. Photochemical ozone formation in the high NO_x regime exceeded that for low NO_x by factors of 2 to 6, whereas O_3 destruction in the low NO_x regime exceeded that for high NO_x by factors of up to 3. Taking the tropopause height to be 17 km, estimates of the net photochemical effect on the O_3 column revealed that the high NO_x regime led to a small net production. By contrast, the low NO_x regime was shown to destroy O_3 at the rate of 3.4% per day. One proposed mechanism for off-setting this projected large deficit would involve the transport of O_3 rich midlatitude air into the tropics. Alternatively, it is suggested that O_3 within the tropics may be overall near self-sustaining with respect to photochemical activity. This scenario would require that some tropical regions, unsampled at the time of PEM-B, display significant net column O_3 production, leading to an overall balanced budget for the "greater" tropical Pacific basin. Details concerning the chemical nature of such regimes are discussed.

1. Introduction

To understand the photochemistry of tropospheric ozone, the distribution of NO and NO_x ($NO+NO_2$) must be understood. It is the cycling of NO_x as facilitated by peroxy radicals that governs the photochemical formation of ozone [*Chameides and Walker*, 1973; *Crutzen*, 1973]. For example, even though both stratospheric-tropospheric exchange and surface deposition contribute to the tropospheric O_3 budget, photochemical formation and destruction typically make much larger contributions to the budget [e.g., *Fishman et al.*, 1979; *Liu et al.*, 1980; *Fehsenfeld and Liu*, 1993; *Davis et al.*, 1996a]. However, considerable uncertainty remains in the quantitative evaluation of these photochemical components, particularly as related to the distribution of NO_x.

Estimating the tropospheric distribution of NO_x presents a significant challenge for several reasons. Among these are the fact that primary sources for this species are very diverse in nature, ranging from surface emissions (both anthropogenic and natural in origin) to lightning, aircraft emissions, and stratospheric injections [e.g., *Hameed et al.*, 1981; *Liu et al.*, 1980; *Logan*, 1983; *Levy and Moxim*, 1989; *Penner et al.*, 1991; *Kasibhatla et al.*, 1991; *Beck et al.*, 1992; *Wuebbles et al.*, 1993; *Davis et al.*, 1996a; *Jacob et al.*, 1992, 1996]. Further complicating this picture is the role played by secondary sources of NO_x. The origin of the latter source involves the chemical recycling of longer-lived nitrogen species such as HNO_3 and PAN as well as other potential NO_y species [e.g., *Liu et al.*, 1987; *Chatfield and Delany*, 1990; *Singh et al.*, 1992; *Jacob et al.*, 1992, 1996; *Davis et al.*, 1996a]. Still further complicating the NO_x distribution picture is the highly

[1]School of Earth and Atmospheric Sciences, Georgia Institute of Technology, Atlanta.

[2]Solar Terrestrial Environmental Laboratory, Nagoya University, Toyokawa, Aichi, Japan.

[3]Graduate School of Oceanography, University of Rhode Island, Narragansett.

[4]NASA Langley Research Center, Hampton, Virginia.

[5]Department of Chemistry, University of California, Irvine.

[6]Institute for the Study of Earth, Oceans, and Space, University of New Hampshire, Durham.

[7]NASA Ames Research Center, Moffet Field, California.

Paper number 97JD00011.
0148-0227/97/97JD-00011$09.00

variable lifetime of this species. This can vary from less than 1 day at BL altitudes to nearly 2 weeks at very high altitudes.

Using source inventory data with different types of models, several groups have undertaken the goal of generating estimates of the global tropospheric NO_x distribution [e.g., *Ehhalt et al.*, 1992; *Kasibhatla et al.*, 1993; *Levy et al.*, 1996]. Unfortunately, the scarcity of observations, especially at high altitudes and in remote areas such as the tropics, have made it difficult to substantiate significant components of these studies. Regional campaigns attempting to obtain measurements of NO and NO_x over a substantial altitude range have included the Stratospheric Ozone III campaign (STRATOZ) [*Drummond et al.*, 1988] and NASA's Global Tropospheric Experiment (GTE). The latter program has encompassed field studies in the Amazon River Basin (Amazon Boundary Layer Experiment (ABLE) 2A and 2B [*Harriss et al.*, 1988, 1990]); the Arctic and sub-Arctic (Arctic Boundary Layer Expedition, ABLE 3A and 3B [*Harriss et al.*, 1992, 1994]); the western North Pacific (Pacific Exploratory Mission (PEM)-West A [*Hoell et al.*,1996]); and the tropical Atlantic (Transport and Atmospheric Chemistry Near the Equatorial Atlantic (TRACE A) [*Fishman et al.*, 1996]). In most cases individual observations during these campaigns have shown large variability in NO levels; however, median values from one region to another have generally exhibited more modest/gradual variations [*J. Bradshaw, manuscript in preparation,* 1996]. By contrast, during PEM-West B, recorded NO values in the tropics exhibited not only large variability in individual NO measurements but also showed large systematic shifts in regional median values, e.g., approaching an order of magnitude on the regional scale. This paper examines the large shift in median NO values in the tropical Pacific. The primary focus will be identifying the factors responsible for this shift and evaluating the photochemical consequences of this shift.

2. Observational Data

2.1. NO and Other Photochemical Measurements

While atmospheric NO measurements over the last decade have shown a trend of increasing reliability [*Hoell et al.*, 1985, 1987, 1996; *Gregory et al.*, 1990], observations from independent instruments still serve to increase one's confidence in unexpected findings. In the case of PEM-West B, measurements were reported by two groups: Georgia Institute of Technology and Nagoya University. The former group used the two-photon laser-induced fluorescence (TP-LIF) technique, while the latter group employed the more common NO detection method of O_3 chemiluminescence. The results from these two approaches compared quite well for all PEM-West B flights. For example, based on 30-s sampling intervals, a standard regression analysis of almost 5000 paired NO measurements gave a regression line having a slope of 1.25 $\pm$ 0.01, an intercept of 1.2 $\pm$ 0.2 pptv, and an R^2 value of 0.95 with Nagoya (the dependent variable) having the higher NO values. Although this comparison only involved data with mixing ratios in the range of 0-200 pptv, these data constituted nearly 99% of the total data set. For further details concerning the experimental hardware and measurement methodology, the reader is referred to *Hoell et al.* [this issue].

The measurement techniques employed for all other critical photochemical parameters (e.g., CO, H_2O, O_3, NMHCs, and UV irradiance) as well as aerosol parameters (e.g., CN and size/# density) have been summarized by *Hoell et al.* [this issue]. Also reported for each of these methodologies are the data sampling rate, precision, accuracy, and nominal limit of detection (LOD).

Since no observed values of NO_2 were recorded during PEM-West B, NO_2 mixing ratios were estimated from photochemical box-model calculations (see later discussion in section 3.2.1.). Thus the values of the photochemical quantity NO_x (NO + NO_2) used throughout this analysis are those estimated from $(NO)_{meas}$ and $(NO_2)_{calc}$.

2.2. Sampling Region

On the basis of meteorological considerations the PEM-B sampling region has been separated into two large regional areas as illustrated in Figure 1. These regions are defined by the large-scale outflow from the Asian continent. Latitudes north of 20°N were heavily impacted by continental outflow [*Merrill, et al.*, this issue]. By contrast, to the south of this latitude and east of 120°E, continental influences were found to be minimal, leading to our tentative conclusion that this region was representative of a remote tropical-marine environment. It is the latter region that exhibited the large shifts in NO and is the focus of this paper. As shown in Figure 2, the remote tropical component of the PEM-B flight track contained all or portions of flights 5-10. During flights 5-8 the free tropospheric mixing ratios of NO were found to be highly elevated (e.g., often in excess of 100 pptv), whereas during flights 9 and 10 levels almost never exceeded 20 pptv. The former sequence of flights will be defined hereafter as the "high" NO_x regime, while the latter flight sequence (i.e., 9 and 10) will be referred to as "low" NO_x. Note also that although geographically in the tropics, the near-coast portions of flight 10 and all of flight 11 (i.e., longitudes west of 120°E) have not been included in this analysis because both showed evidence of having been significantly influenced by low and medium

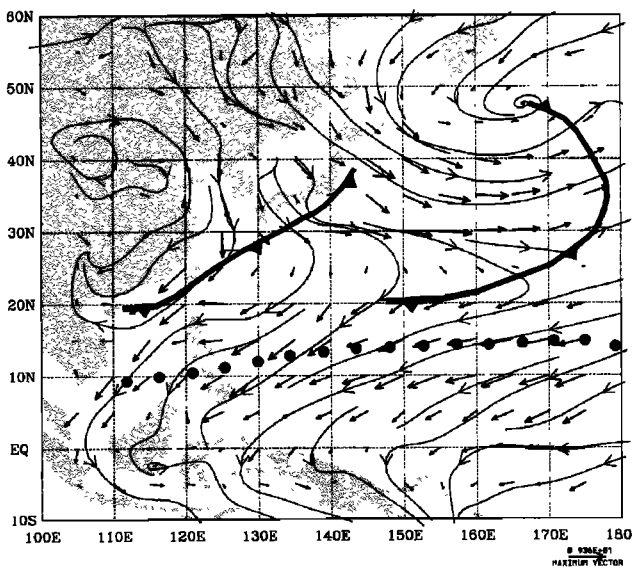

Figure 1. Overview of mean winds and synoptic conditions during the PEM-West B sampling period. Also shown are primary cold frontal zones with the dotted line representing the southernmost extent of cold frontal movement during PEM-West B.

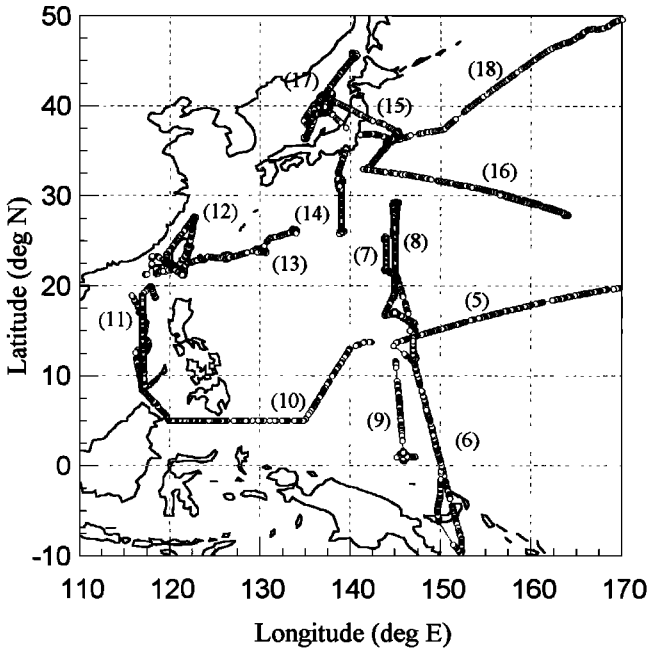

Figure 2. PEM-West B data collection region. Flight numbers are shown in parentheses. Circular symbols indicate individual in situ measurements of NO.

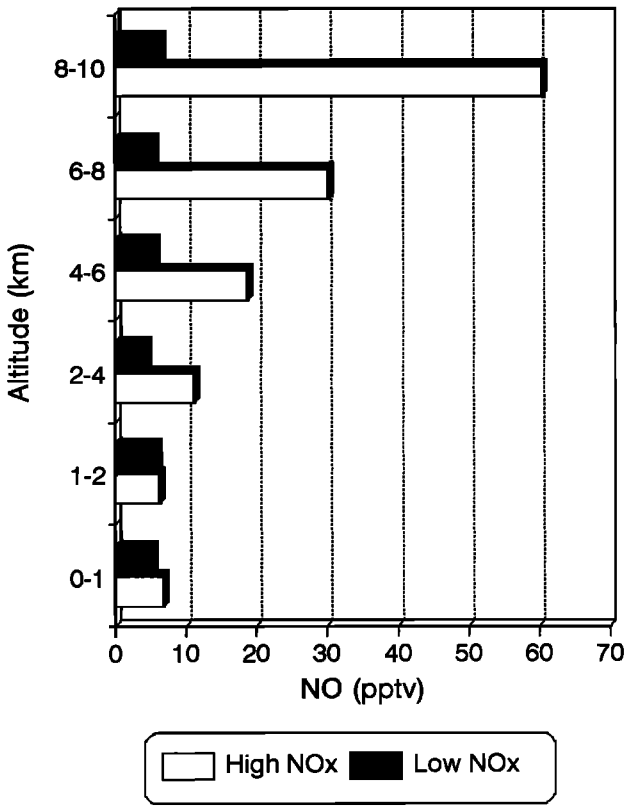

Figure 3. High and low NO_x regime NO altitude distributions. Median values were derived from data binned into 1 km increments from 0-2 km and 2 km increments from 2-10 km.

altitude continental outflow, e.g., CO levels often in excess of 200 pptv. *Talbot et al.* [this issue] have also examined the tropical PEM-B region in terms of continental and aged marine air masses. While their designations are in many ways similar to ours, differences exist since their data separation is based predominantly on isentropic trajectories; also, they include those portions of flights 10 and 11 that we have omitted.

In order to facilitate a statistical comparison of the two regimes, all flight data falling within a solar zenith angle window of 0-60° were grouped into altitude bins of 0-1, 1-2, 2-4, 4-6, 6-8, and 8-10 km. Comparisons between regimes therefore are based on median conditions for each altitude block for each regime. Table 1 presents the distribution of data available for this analysis. In this case, the number of data points (i.e., 30-s averages) as well as the number of flights contributing data are listed for each altitude block in each regime. Since the high NO_x regime had more flights that contributed data, this regime is clearly more robust than the low NO_x regime. For example, only for the altitude range of 8-10 km are both regimes nearly equal in terms of total available data. This can be largely attributed to the fact that low "NO_x" flight 10 sampled almost exclusively at 9.5 km between 120° and 145°E. Strictly speaking, therefore, the flight map shown in Figure 2 should be viewed as primarily providing the geographical range spanned by both regimes at high altitudes (i.e., 8-10 km). For lower altitudes the in situ data for the two regimes are more restricted as the bulk of these data come from a longitudinal band spanning 143-153°E.

Table 1. Distribution of Data in the High and Low NO_x Regimes

Altitude Range, km	High NO_x		Low NO_x	
	Flights	Data pts.	Flights	Data pts.
0-1	6,7,8	80	9	57
1-2	6,7,8	18	9,10	14
2-4	5,6,7,8	77	9,10	27
4-6	5,6,7,8	224	9,10	27
6-8	5,6,7	185	9,10	29
8-10	5,6,7,8	561	9,10	405

Figure 3 shows a comparison of median NO mixing ratios as a function of altitude for the "high" and "low" NO_x regimes. These result show that NO levels are considerably larger for the high NO_x regime at all free tropospheric altitudes. The difference between the two regimes is seen to range from a factor of 2.5 for altitudes of 2-4 km to nearly 1 order of magnitude (e.g., 6 versus 60 pptv) at altitudes of 8-10 km. Quite noteworthy also is the observation that for all altitude blocks above 2 km the median values for the two regimes differ by more than one quartile. Interestingly, NO levels for the low NO_x regime remain essentially constant with altitude; therefore, the large differences observed between the two regimes at the higher altitudes are seen to be entirely due to increases in NO in the high NO_x regime.

As shown in Figure 4, the trends in NO_x deviate only slightly from those shown for NO in Figure 3. The steady increase of NO_x with altitude in the high NO_x regime is similar to the trend for NO but is somewhat less pronounced since at low altitudes there is a significant amount of NO_x present as NO_2. At the higher altitudes, NO_x is predominantly in the form of NO due to a significant decrease in the reaction rate between NO and O_3 and a modest increase in the rate of NO_2 photolysis. In sharp contrast to the NO_x profiles shown for the high NO_x re-

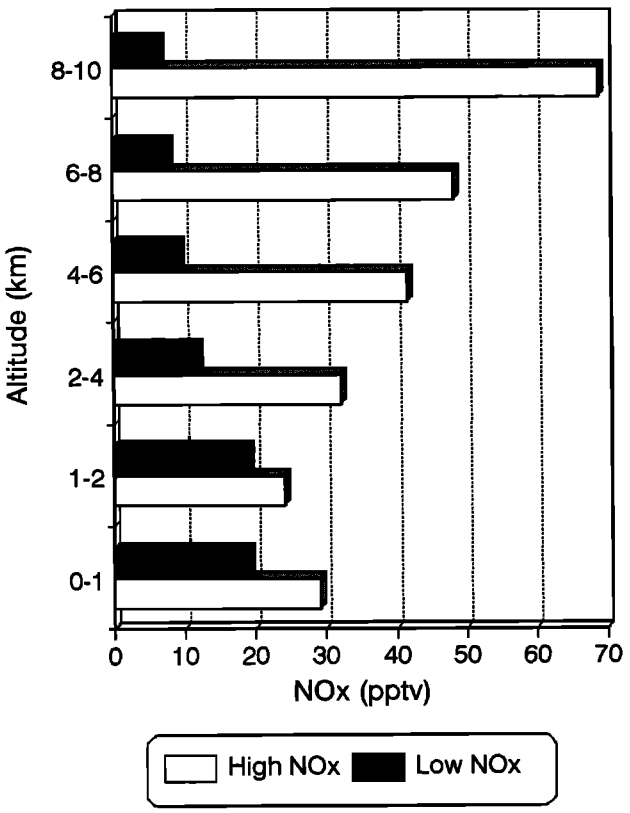

Figure 4. High and low NO_x regime NO_x altitude distributions. Calculated median values were derived from data binned into 1 km increments from 0-2 km and 2 km increments from 2-10 km.

gime, levels slowly decrease with altitude for low NO_x. Thus at 8-10 km the difference in NO_x also reaches 1 order of magnitude (e.g., 7 versus 70 pptv).

2.3. Back Trajectories and Chemical Tracers

To further explore the key factors responsible for the tropical shift in NO_x, both back trajectories and chemical tracers were examined. This analysis included all flights listed earlier in the text as being identified with either the high or the low NO_x regimes. Representative trajectories are presented in Figure 5, and chemical tracer data are presented in Figures 6a-6f.

2.3.1. Back trajectories. Back trajectories can provide some indication of both where a sampled air mass may have originated and how that parcel may have been influenced as it tracked to the point of sampling. Shown in Figure 5 are several 10 day isentropic back trajectories for selected air parcels. (Note that the symbols at the end of each trajectory indicate the location of the aircraft at the time of sampling.) In this case, because of the higher density of data in the 8-10 km range and the fact that the difference in the NO mixing ratio was largest at this altitude, the trajectories shown are based on aircraft locations within 8-10 km. From Figure 5 it is quite apparent that the source regions for the two regimes are distinctly different. For example, high NO levels are primarily associated with trajectories that are confined to the northern hemisphere. This is true not only for those trajectories shown in Figure 5 but for all isentropic trajectories calculated for altitudes above 2 km. Furthermore, approximately 80% of the trajectories for the high NO_x regime are indicated to have recently passed over the Asian continent (i.e., within 2-3 days of sampling). By contrast, the trajectories associated with the low NO_x regime are seen as being exclusively from the southern hemisphere. Again, this is not only true for the examples shown in Figure 5 but for all trajectories above 2 km. Approximately 50% of the low NO_x trajectories track back to remote South Pacific points of origin. The remaining 50%, although from the southern hemisphere, pass over New Guinea.

For purposes of comparison with the isentropic trajectories of Figure 5, a set of 6 day kinematic trajectories were provided by S. McKeen (private communication, 1996). For both regimes, these trajectories tended to travel more slowly covering roughly half the distance of the isentropic trajectories per day. For the high NO_x regime the two methods compared quite well. Both indicated air parcels being transported eastward from southeastern Asia at high altitude. In the case of low NO_x the kinematic trajectories differed somewhat in that they did not cross the equator or remain at high altitude. Instead, air parcels were shown rising steadily from altitudes as low as 2 km while at the same time being transported westward from the tropical, central Pacific. Thus the kinematic trajectories offer a somewhat different perspective on the origin of the air parcels sampled in the low NO_x regime; however, they do not alter the earlier conclusion, based on the isentropic trajectories, that this regime was predominantly influenced by marine sources.

While back trajectories are much less reliable for BL conditions, especially after more than 2 days, it is still noteworthy that near-surface isentropic trajectories do not follow the pattern of those in the free troposphere. For both regimes, most of the trajectories have the central North Pacific as a source region.

2.3.2. Chemical tracers. As noted above, chemical tracer data can also be an indicator of the origin and/or history of a sampled air parcel. With the notable exceptions of NO_x and O_3 the source of many chemical tracers at high altitudes is the direct result of the coupling between vertical transport and the release of a species at or near the surface. In these cases, one of the more important vertical mixing processes can be deep convection. During PEM-B the tropics was convectively quite active as evidenced by numerous visual as well as satellite observations. Evidence supporting the notion that deep convection was indeed important in the redistribution of several tracers can be found in many of their altitude profiles. As illustrative of this, Figure 6a shows median values versus altitude for "fine" aerosol particles as expressed as CN (condensation nuclei) number density. These data clearly indicate that for both the high and the low NO_x regimes, median CN values significantly increase with altitude. As suggested by other investigators [*Clarke et al.*, 1993; *Thornton et al.*, 1996] a likely explanation for this observation is that for tropical conditions, significant amounts of volatile surface sulfur (e.g., volcanic, anthropogenic, and/or biogenic) are pumped to high altitudes via deep convection. At high altitudes this reduced sulfur can be oxidized by OH radicals, and the resulting sulfuric acid, at very cold temperatures and in the absence of significant populations of larger particles, leads to the formation of new particles via nucleation processes. Thus, these data support the hypothesis that both the high and the low NO_x regimes experienced the effects of deep convection. That deep convection occurring over both environments could lead to elevated high-altitude sulfur levels and hence CN levels is

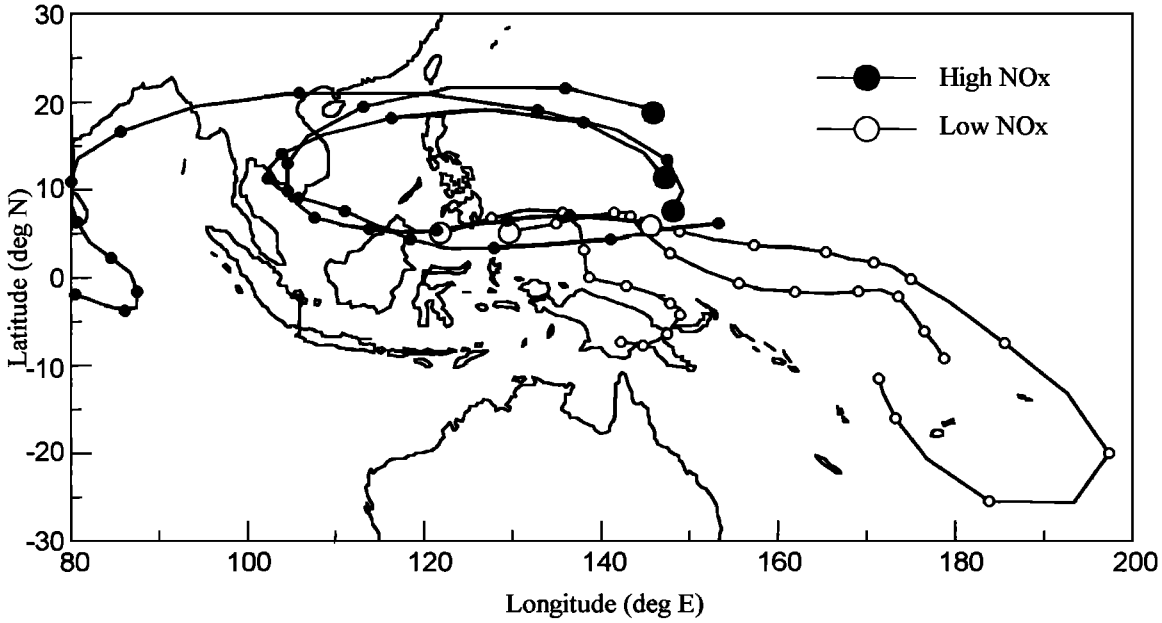

Figure 5. Selected isentropic back trajectories representative of the high and low NO_x regimes. Trajectories are for altitudes between 8 and 10 km. Large circles indicate the location of the aircraft at the time of sampling. Trajectories extend backward in time 10 days with each day represented by the distance between the smaller circles.

not all that surprising since significant sulfur sources exist over both continental and marine regions of the tropics.

Other chemical tracers can help point toward whether the convection was over continental or marine regions. For example, CH_3I is considered an excellent tracer for BL marine air. This species has predominantly an ocean source and its lifetime is only a day or two in the tropics [*Chameides and Davis*, 1980; *Solomon et al.*, 1995; *Davis et al.*, 1996b; *Chen et al.*, 1996]. As shown in Figure 6b, the altitude distribution of CH_3I for the low NO_x regime shows a significant enhancement over that for the high NO_x case. At 8-10 km this results in median CH_3I mixing ratios that are more than twice that for the high NO_x regime. In fact, for all altitudes above 2 km, the lower quartile for the low NO_x regime exceeds the upper quartile value for the high NO_x. These results thus are consistent with the hypothesis that the low NO_x regime was more heavily influenced by marine convection. Although dimethylsulfide (DMS) might also be considered as a useful tracer of marine convection, the measured median concentration levels for this species were found to be too near the limit of detection (LOD) to justify a detailed quantitative comparison between the two regimes. Even so, quite relevant to the above argument were those DMS observations recorded for the highest-altitude data bin at 8-10 km. In this case, the upper quartile value for the low NO_x regime was nearly a factor of 3 higher than the LOD for DMS. By comparison, the high NO_x upper quartile DMS value was still at the LOD level. Thus the DMS results are qualitatively consistent with those for CH_3I.

Just as CH_3I and DMS may be viewed as excellent tracers of marine BL air, CO and NMHCs can be considered equally good tracers of surface continental air. As shown in Figure 6c the median values for CO versus altitude indicate that above 2 km the difference between the two NO_x regimes averages less than 7 ppbv and never exceeds 11 ppbv. Not surprisingly, the respective median values also fall within one quartile of each other. Thus these results suggest that neither regime was preferentially influenced by continental emissions. The median levels for the high and low NO_x regimes (i.e., ranging from 83 to 97 ppbv) would also argue that the source strength of CO from combustion that had been advected into both regions was relatively low. However, in contrast to CO the results for several NMHC species did show a systematic difference. A likely reason for this is that the latter species have very low background levels in the upper atmosphere relative to CO. This characteristic can be attributed to their having typically shorter atmospheric lifetimes versus CO and their having sources which are limited to the surface only. As illustrated in Figure 6d, a significant difference is seen in the mixing ratios of C_3H_8 for the two regimes. Differences between 4-8 km are larger than one quartile; but for the 8-10 km range, where C_3H_8 is roughly 1.5 times higher for high NO_x, median values actually fall within one quartile. This reflects the greater variability in C_3H_8 levels at high altitude as one might expect due to its short lifetime and surface source. Differences reflecting a similar trend were also observed for the NMHC species C_2H_6, C_2H_2, and C_6H_6.

Lead 210 and the organic acids HC(O)OH and $CH_3C(O)OH$ represent still other tracers that can be associated with surface continental sources [*Dibb et al.*, this issue]. Quite significant in this case is the fact that ^{210}Pb is the daughter of ^{222}Rn, a species naturally emitted mainly over continental areas. As shown in Figure 6e, the high NO_x regime clearly shows a much stronger influence from continental sources than the low NO_x regime. (The authors note that the sparseness of this database reflects the long integration times required for the low levels of ^{210}Pb.) In the case of the organic acids, although only a 20% difference was found in the levels of HC(O)OH, for $CH_3C(O)OH$ the trend observed at high altitudes was similar to

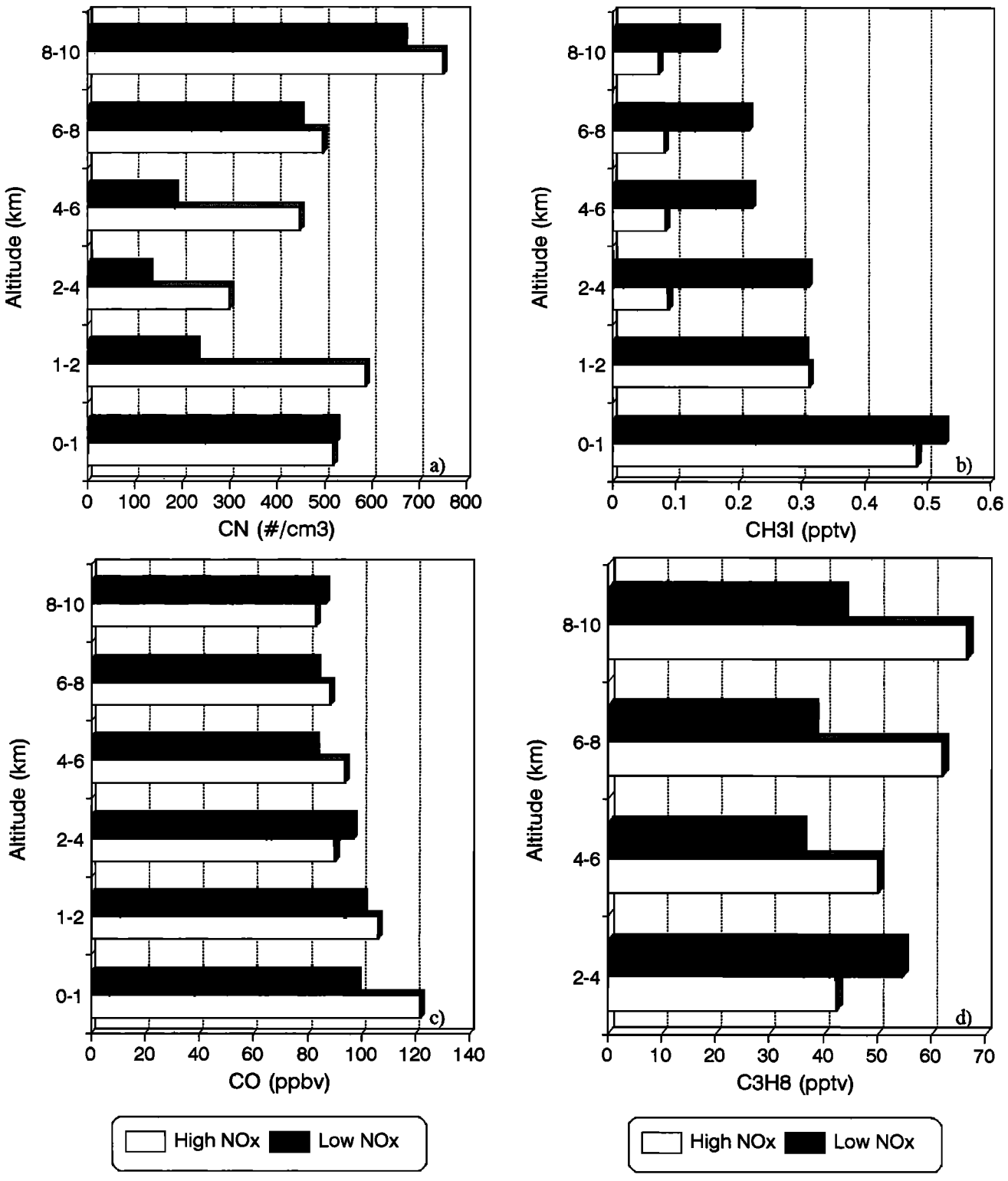

Figure 6. High and low NO_x regime altitude distributions for (a) CN, (b) CH_3I, (c) CO, (d) C_3H_8 and (f) O_3. Median values were derived from data binned into 1 km increments from 0-2 km and 2 km increments from 2-10 km. Figure 6e is a scatterplot of ^{210}Pb versus altitude for the high and low NO_x regimes.

that for ^{210}Pb in that the high NO_x regime showed significantly higher levels, on the average being nearly a factor of 2 larger than those recorded for low NO_x.

O_3 is typically not considered a simple tracer of either continental or marine surface air because of its high photochemical reactivity and its highly variable mixing ratio as a function of altitude. In cases, however, where independent data suggest that a given air parcel was influenced by deep convection over a marine region versus having been more influenced by deep convection over a continental area, some

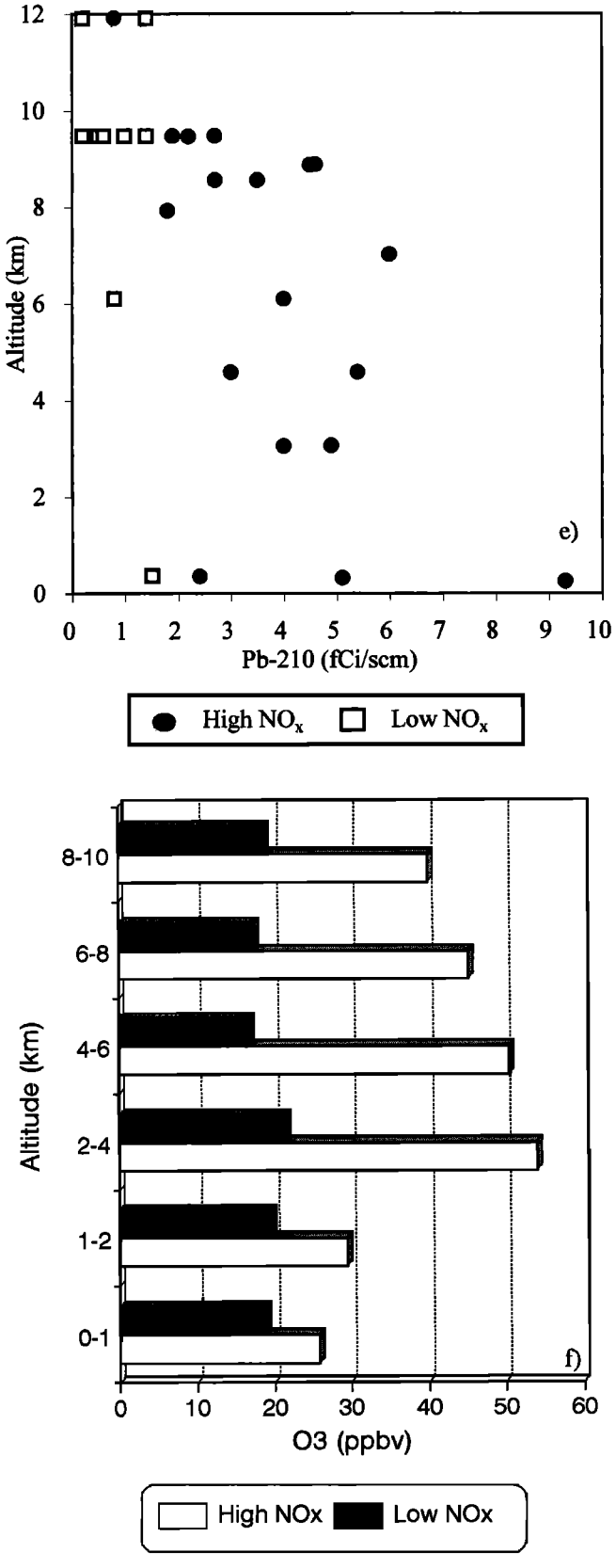

Figure 6. (continued)

general arguments can be developed concerning the type of O_3 profile that might be observed. For example, in the context of strong vertical mixing over a remote tropical-marine region, transport of air out of the marine BL (where photochemical destruction of O_3 dominates formation) would most likely lead to rather low and uniform levels of O_3 at all altitudes. By contrast, because of elevated levels of NO_x and hence a tendency toward net photochemical O_3 production, continental BL air transported to high altitudes and then advected out over the ocean would tend to generate less uniformity in O_3 levels and most likely lead to higher than average levels of free tropospheric O_3. As shown in Figure 6f, low uniform levels of ozone observed in the low NO_x regime are consistent with a picture involving marine convection of BL air. For the high NO_x case, elevated and nonuniform O_3 levels are observed. Ozone profiles similar to those of the low NO_x regime were also found in the tropical Pacific during AASE 2 (Airborne Arctic Stratospheric Expedition) [*Folkins et al.*, 1995], PEM-West A [*Davis et al.*, 1996a], and CEPEX (Central Equatorial Pacific Experiment) [*Kley et al.*, 1996]. These investigators also attributed their observations to deep convection over a marine region involving O_3 poor BL air.

3. Discussion

3.1. Origin of NO_x Sources

The back trajectories and chemical tracer data have shown that while there are a few similarities between the low and the high NO_x regimes, there are far more dissimilarities. These differences can be most easily understood in terms of the impact of deep convection in relationship to source regions. The isentropic back trajectories indicate that much of the air associated with the low NO_x regime remained over the tropical South Pacific for several days before crossing the Intertropical Convergence Zone (ITCZ) and entering the northern hemisphere. While kinematic trajectories do not cross the ITCZ, they do indicate rising air transported westward from remote parts of the tropical central Pacific. The tracer species CH_3I also provides evidence indicating a preponderance of marine convection in this regime. For instance, at altitudes of 8-10 km the low NO_x regime had CH_3I levels more than twice as high as that recorded for the high NO_x. (For comparison purposes, BL values of CH_3I in both the high and the low NO_x regimes were within 20% of each other and were also within a similar margin of the tropical CH_3I data from PEM-A.)

Observations in the high NO_x regime, by contrast, suggest the strong influence of deep convection over a landmass. In this case, the isentropic trajectories were all positioned in the northern hemisphere, and 80% of these trajectories indicate that the parcel had passed over a land mass within 2-3 days of the sampling time. The kinematic and isentropic trajectories were found to be in good agreement. Tracers of continental origin (i.e., NMHCs, ^{210}Pb, and organic acids) also suggest a significant degree of interaction between the surface and the upper free troposphere.

Collectively, the above results suggest that two distinctively different surface environments, via deep convection, mixing, and transport, resulted in dramatically different impacts on what have been labeled here as high and low NO_x regimes. It is centrally important to differentiate between these two environments since their influence on free tropospheric levels of NO_x could be expected to be quite different. Not only would they differ in the levels of NO_x that might be transported out of the boundary layer, but they could also differ significantly in the expected level of electrical activity and hence lightning generated NO_x. As shown in previous lightning-flash satellite data [*Turman and Edgar*, 1982; *Orville and Henderson*, 1986;

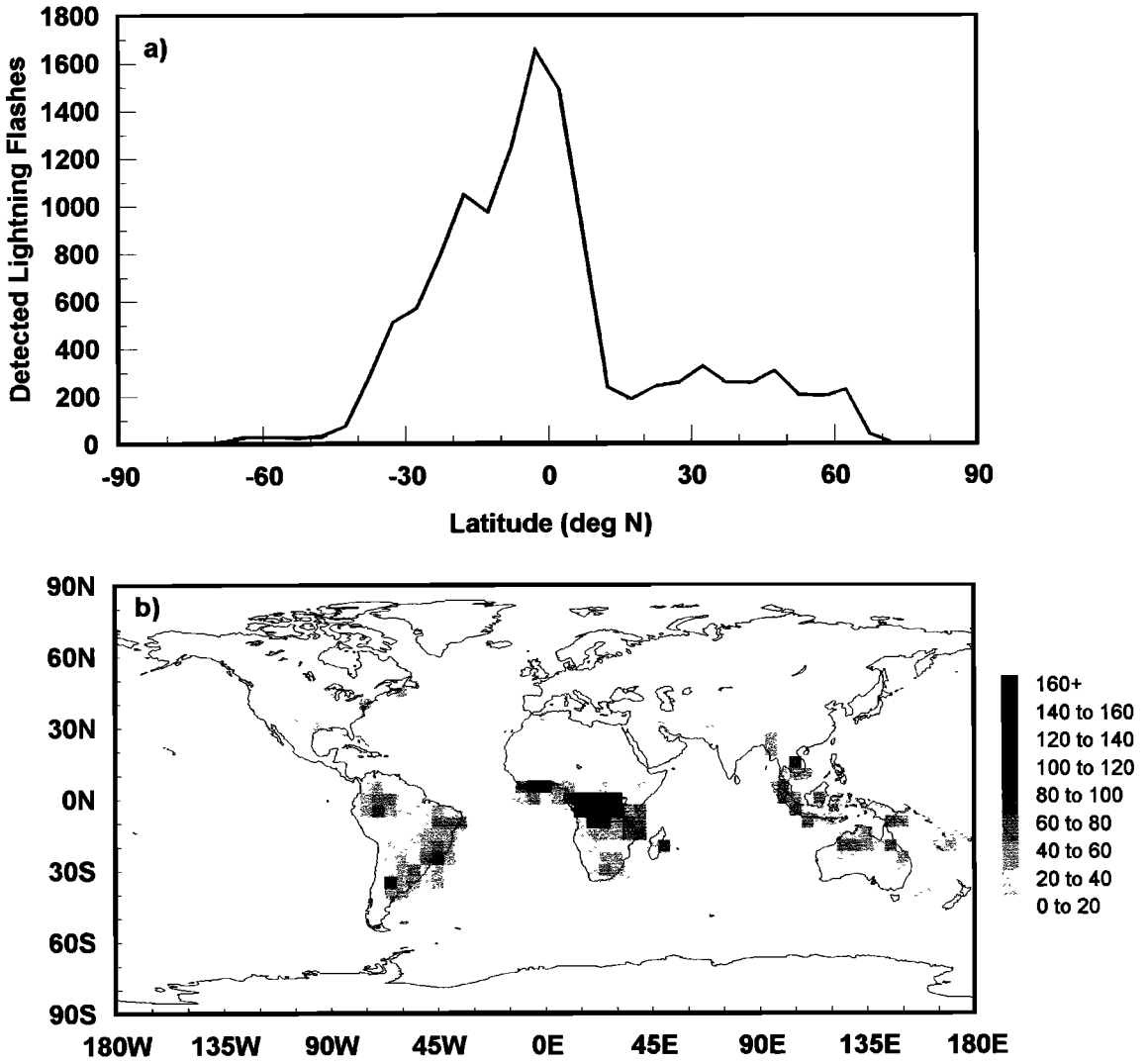

Figure 7. (a) Latitudinal frequency distribution of lightning flashes derived from DMSP OLS data for February and March, 1994; (b) geographical distribution of DMSP OLS lightning flash data for February and March 1994.

Goodman and Christian, 1993], marine convection is generally associated with much lower levels of electrical activity than continental convection, leading to the expectation of smaller contributions of NO_x from lightning in the low NO_x regime.

In the absence of both lightning generated NO_x and a surface source of this species, one would expect marine convection to pump rather low levels of NO_x from BL altitudes to the upper free troposphere [e.g., *McFarland et al.*, 1979; *Thompson et al.*, 1993; *Davis et al.*, 1987, 1996a]. In contrast to the minimal NO_x effects from deep convection over marine areas, deep convection over a continental land mass can influence NO_x by both lightning and vertical transport of surface emissions. During PEM-B the potential impact from lightning can be seen in the form of Figures 7a and 7b. Figure 7a shows a latitudinal lightning frequency distribution for the months of February and March 1994 (S. Goodman, NASA Marshall Space Flight Center and the University of Colorado, unpublished data). These data were derived from the near local midnight (1030-1130) passes of the Defense Meteorological Satellite (DMSP) based on the F10 satellite optical linescan system (OLS) visible band imagery. This distribution shows a maximum of about 1600 lightning flashes near the equator. (Note that the DMSP OLS system detects only a small fraction of the total lightning (e.g., 2% or less), but over the course of 1 month provides a reasonably realistic depiction of the most active thunderstorm regions [*Goodman and Christian*, 1993].) While falling off more rapidly in the northern hemisphere, it is quite noteworthy that the latitude range of 0-15°N still shows lightning flash levels that are nearly as intense as those in the southern hemisphere. Nevertheless, as discussed earlier, the effects from this distribution do not show up in the form of elevated NO values for the low NO_x regime. This apparent inconsistency largely disappears when the geographical distribution of the DMSP lightning data is considered. For example, as shown in Figure 7b those regions having the highest flash density in both the northern and the southern hemispheres are those located near significant landmasses. The lowest flash rates are seen for areas far removed from land over the open Pacific. The latter setting is indicated in over half of the low NO_x isentropic back trajectories, whereas nearly 80%

of the high NO_x regime isentropic trajectories involve passage over an extensive landmass.

Although the DMSP lightning flash data together with trajectory and tracer data suggest that a major source of NO_x in the high NO_x regime could have been lightning, the possible contribution from surface emissions still requires some investigation. In the text that follows we explore this question from several points of view. The first of these involves the observed trends in the trace gas CO. Recall that earlier in the text, when presenting the comparison of CO values, we found only a very modest difference between the two regimes. If surface combustion were a significant contributor to the elevated levels of NO_x, one might expect that the difference in CO levels between regimes should have been much larger. On the other hand, the fact that there were significant differences recorded in the levels of C_3H_8 at high altitudes does suggest some contribution from surface emissions. In an effort to semiquantitatively evaluate the possible magnitude of this source, we have used the ratio of C_3H_8 to NO_x as reported by *Davis et al.* [1996a]. These authors have suggested that under certain conditions this ratio can provide an upper limit estimate of the NO_x fraction attributable to surface emissions when the analysis is confined to one to two NO_x lifetimes downwind of the emission source. Davis et al. uses a BL value of 3:1 $\pm$ 1 in their analysis of the PEM-A data [*Davis et al.*, 1996a]. This value is based on observations of C_3H_8/NO_x downwind of urban/industrialized areas in the PEM-A sampling region as well as on observations downwind of urban areas in the southeastern United States.

Recently, a more extensive examination of C_3H_8/NO_x data for PEM-A as well as PEM-B and the GTE program TRACE A has shown that the 3:1 value for this ratio does not apply to regions where NMHC sources are dominated by biomass burning (e.g., the South Atlantic during the burning season). In this case, the partitioning of hydrocarbons is shifted away from that observed from high temperature combustion sources as evidenced by the ratios of C_3H_8/C_2H_6, C_3H_8/C_2H_2, and C_3H_8/C_6H_6. On the basis of industrial emissions near Atlanta, Georgia [*Jeffries*, 1995], these ratios are expected to be around 0.75, 2.0, and 4.5, respectively. In fresh biomass burning plumes sampled during TRACE A, these ratios were 0.2, 0.5, and 1.2, respectively, indicating that biomass burning emissions contain a much smaller fraction of C_3H_8. Complicating things still further is the fact that NO_x levels from biomass burning can be largely controlled by nitrogen tied up chemically within the biomass.

It was also found that for colder conditions such as those encountered at extratropical latitudes (i.e., >20°N) during PEM-B, the reservoir species PAN (peroxyacetylnitrate) can chemically tie up a very large fraction of the emitted NO_x. This leads to elevated values for the C_3H_8/NO_x ratio at the surface; and thus a more appropriate surface ratio needs to include PAN, i.e., $C_3H_8/(NO_x + PAN)$. Quite significantly, the high NO_x regime of PEM-B suffers from neither of these potentially serious difficulties as emissions were found to be predominantly industrial in nature and the warm temperatures preclude high PAN levels. Given these caveats and again assuming a downwind surface value for the C_3H_8/NO_x ratio of 3:1, the high altitude values of C_3H_8 (i.e., 65 pptv) and of NO_x (i.e., 70 pptv) suggest that no more than one third of the high altitude NO_x in the high NO_x regime was due to transport of surface NO_x emissions. Thus it could be argued that two thirds or more of the NO_x was due to lightning.

Yet a different explanation for the excess NO_x, NO_x above and beyond that estimated from the surface, might be the recycling of NO_y species (i.e., $NO_y = NO + NO_2 + HNO_3 + PAN + HONO_2 + N_2O_5$ + other organic nitrates). Use of the C_3H_8/NO_x ratio assumes that the photochemical lifetime of NO_x is shorter than that for C_3H_8. If so, use of the 3:1 ratio or a value close to this tends to provide an upper limit for the amount of surface NO_x. However, in the event of significant recycling of NO_x from reservoir NO_y species (e.g., HNO_3, PAN, etc.) the atmospheric residence time of NO_x could approach or exceed that of C_3H_8. Under these conditions, high altitude NO_x levels could also end up being elevated relative to that expected from surface emissions. For the high NO_x regime, though, the observed 148 pptv of HNO_3 and 55 pptv of PAN could only explain approximately 20-30% of the NO_x. Even so, we cannot at this time totally rule out the possibility of either yet unidentified recycling pathways (e.g., other than photolysis and reaction with OH) or the presence of yet unidentified NO_y species, both of which might lead to the additional generation of recycled NO_x. Some investigators, in fact, have concluded that recycling played a major role in the NO_x budget in the tropical South Atlantic during NASA's TRACE A field study [e.g., *Jacob et al.*, 1996; *Smyth et al.*, 1996]. Possible mechanisms by which more rapid recycling of NO_x might take place have been proposed by *Chatfield* [1994] and *Fan et al.* [1994] and have encompassed heterogeneous reactions involving HNO_3 and CH_2O.

During PEM-B median HNO_3 mixing ratios in the high NO_x regime exceed those in low NO_x by only about a factor of 2. By contrast, median PAN levels above 4 km ranged from 5 to 10 pptv in the low NO_x regime but reached levels of 50-65 pptv for high NO_x. Thus given the small difference in HNO_3 and the large difference in PAN, it could be argued that other organic nitrate species were transported with the PAN and might have been responsible for the observed high NO_x mixing ratios as a result of recycling. While we acknowledge this possibility, we believe that a far more plausible explanation for the elevated NO_x is that it was simply the product of lightning and that the NO_x had not yet fully converted to HNO_3. Recall that isen-tropic trajectories indicate that most of the air parcels had come from the western Pacific Rim only 2-3 days back in time. The calculated lifetime of NO_x for conversion to HNO_3 above 4 km is of the order of 3-9 days.

A recent global modeling study of lightning [*Levy et al.*, 1996] adds further support to the authors' position regarding lightning as the major source of NO_x. *Levy et al.* used a 3-D global chemistry and transport model to evaluate the role of lightning. Their approach involved estimating the global NO_x distribution generated from nonlightning sources followed by a comparison of this distribution with observations from major field studies, including PEM-A. The lightning contribution was assigned from the difference between observations and the model-estimated NO_x distribution. This study set the annual global NO_x source strength from lightning at between 2 and 6 TgN. Assuming a median global value of 3 TgN/y, *Levy et al.'s* results suggest that even during winter months lightning would contribute from 50 to 80% of all upper tropospheric NO_x in the tropical North Pacific.

In another study, *Kumar et al.* [1995] estimated the global distribution of NO based on satellite lightning sensor data (Ionospheric Sounding Satellite, ISS-b) and theoretical estimates of the lightning production rate as estimated by *Borucki and Chameides* [1984]. The product from this exercise was a

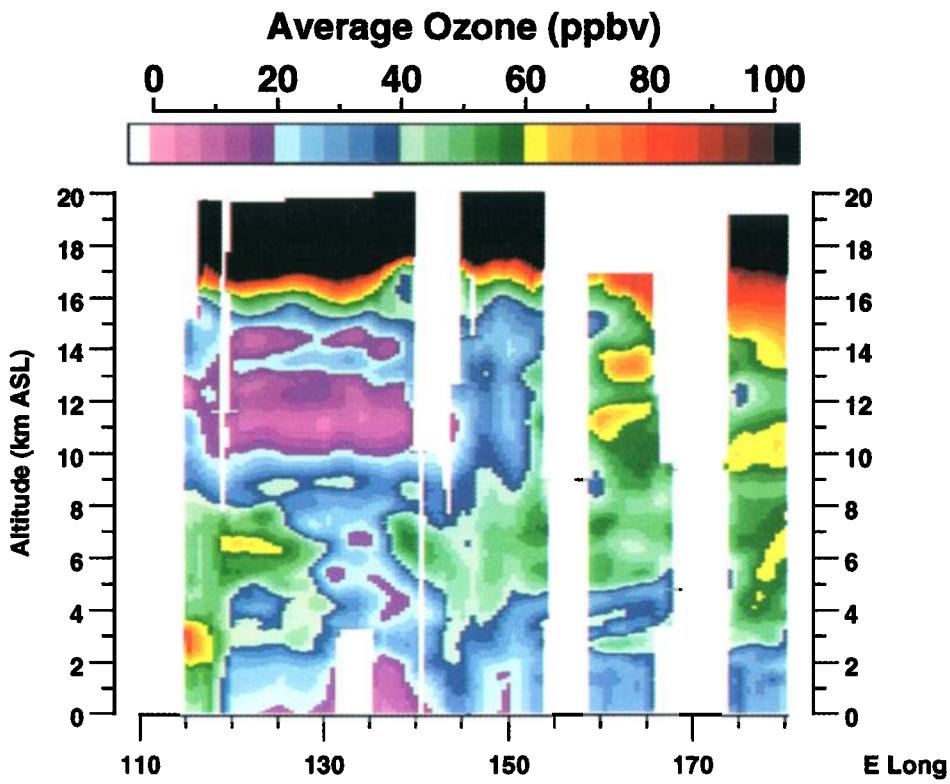

Plate 1. Composite UV DIAL altitude-longitude O_3 distribution based on data recorded between the latitudes 20°N and 10°S. Low altitude values (below 1.5 km) were extrapolated to the surface using in situ O_3 data.

seasonally adjusted global distribution for NO from lightning. For the period of December to February the most significant region of NO production in the northern hemisphere was that located in the tropics over southeastern Asia and Indonesia. Recall that nearly 80% of the trajectories associated with the high NO_x regime passed through this region.

While an understanding of the large-scale tropical processes driving the NO_x shift is of considerable importance, equally important is the closely coupled question concerning which of these regimes might be the dominant one in the tropical-western North Pacific. This issue is particularly important in the context of global modeling efforts that require a "representative" tropical NO_x database. In this context, even though the high NO_x regime was found to be much more robust in terms of the number of flights and amount of data (see Table 1), one cannot assume that this equates to this regime being temporally and/or spatially the most dominant. To further illustrate this point, Plate 1 shows the longitudinal distribution of O_3 at low latitudes (20°N to 10°S) as derived from UV DIAL data and supplemented by more limited in situ O_3 data, particularly that in the marine BL. This represents the most robust spatial coverage obtainable for any constituent measured during PEM-West B. While there is some longitudinal overlap between the high and the low NO_x regimes as described earlier, it is still rather apparent from these data that there is a significant reduction in O_3 levels at nearly all altitudes west of 140°E, a picture that is consistent with Figure 6f. This represents the best evidence available, which suggests that the two NO_x regimes did span a longitudinal band at altitudes below 8 km which was comparable with that at 8-10 km where the bulk of the in situ data was recorded. In fact, it is quite possible that these two regimes persisted in their respective regional dimensions for the duration of the tropical sampling time period; but it is also possible that temporal changes did occur. For example, sampling of the high NO_x regime took place over the time period of February 8-17, 1994, and that for the low NO_x was February 19-21, 1994. Thus it is also possible that each NO_x regime spatially spanned the entire tropical-western North Pacific sampling region during its respective time period. Quite obviously, it is also possible that the real answer involved some combination of spatial and temporal separation. Further exploration of this important issue should be a target for future field programs in the tropical Pacific.

3.2. Ozone Photochemistry

Radical formation in the troposphere is initiated by the photolysis of O_3 in the wavelength range 290-320 nm.

(R1) $O_3 + h\nu \rightarrow O(^1D) + O_2$

Most of the $O(^1D)$ produced in (R1) is collisionally quenched to form $O(^3P)$. This $O(^3P)$ then recombines with O_2 to reform O_3.

(R2) $O(^3P) + O_2 \rightarrow O_3$

Most importantly, a small portion of the $O(^1D)$ also reacts with water to produce hydroxyl radicals.

(R3) $O(^1D) + H_2O \rightarrow 2OH$

While (R3) represents the loss of an O_3 molecule, it also leads to a recycling of radicals that can result in both formation and further destruction of O_3 molecules. For example, the oxidation of CO, CH_4, and nonmethane hydrocarbons (NMHCs) via OH leads to the formation of the peroxy radical species HO_2, CH_3O_2, and RO_2 ($R=C_2H_5$ and higher organic groupings). These peroxy radical species may then react with NO to produce NO_2.

(R4) $HO_2 + NO \rightarrow NO_2 + OH$

(R5) $CH_3O_2 + NO \rightarrow NO_2 + CH_3O$

(R6) $RO_2 + NO \rightarrow NO_2 + RO$

The resulting product NO_2 rapidly photolyzes to produce $O(^3P)$ which combines with an oxygen molecule to produce O_3 as in (R2).

While (R4)-(R6) lead to the formation of O_3, further destruction of O_3 can take place by reaction of O_3 with OH and HO_2.

(R7) $O_3 + OH \rightarrow HO_2 + O_2$

(R8) $O_3 + HO_2 \rightarrow OH + 2O_2$

Still another fate for peroxy radicals is self-reaction, (R9). This process becomes particularly important in regions of low NO.

(R9) $HO_2 + HO_2 \rightarrow H_2O_2 + O_2$

On the basis of reaction sequences listed above, the photochemical formation and destruction of ozone ($F(O_3)$ and $D(O_3)$) can be defined as

$$F(O_3) = \{k_4[HO_2] + k_5[CH_3O_2] + k_6[RO_2]\}[NO] \quad (1)$$

$$D(O_3) = k_3[O(^1D)][H_2O] + \{k_7[OH] + k_8[HO_2]\}[O_3] \quad (2)$$

These expressions clearly indicate the importance of both NO and H_2O in determining the balance between photochemical formation and destruction of O_3. The net effect of all photochemical processes on O_3 (the photochemical ozone tendency) can then be defined as the difference between formation and destruction.

$$P(O_3) = (\{k_4[HO_2] + k_5[CH_3O_2] + k_6[RO_2]\}[NO]) - (k_3[O(^1D)][H_2O] + \{k_7[OH] + k_8[HO_2]\}[O_3]) \quad (3)$$

It should be noted that equation (3) is most appropriate for remote global regions involving low to modest levels of NO_x. As noted by other authors [e.g., *Chameides et al.*, 1987; *Liu*, 1977], under these conditions the additional O_3 loss reaction sequence such as (R10) and (R11) is insignificant:

(R10) $NO + O_3 \rightarrow NO_2 + O_2$

(R11) $NO_2 + OH + M \rightarrow HNO_3$

For the PEM-B high/low NO_x data set, the effect was typically less than 1%.

3.2.1. Model description. As suggested by reactions (R4)-(R6), the photochemical consequences of the shift in NO levels is most directly seen in the O_3 budget. This has been explored in the text that follows using the output from a time dependent (TD) photochemical box model. The model employed has been previously described by *Davis et al.* [1993, 1996a]. The current model differs from that discussed by *Davis et al.* only in the manner in which NO_x sinks and sources were handled. In earlier applications the only sink for NO_x was the daytime reaction of NO_2 with OH. Accordingly, the NO_x source flux was turned on only during daylight hours to avoid a buildup of NO_x during the night. In the current model a 24-hour source flux of NO is assumed since nighttime NO_x sinks have also been included involving the loss of NO_3 and N_2O_5 to aerosols (see, for example, *Ehhalt and Drummond*, 1982; *Liu et al.*, 1987; *Dentener and Crutzen*, 1993) as well as hydrolysis of N_2O_5. Aerosol losses are calculated based on a mass accommodation coefficient of 0.1 for both NO_3 and N_2O_5 [*Dentener and Crutzen*, 1993] and a surface area based on CN measurements (0.01-1 μm) and FSSP-300 aerosol measurements (0.35-20 μm size resolved into 30 bins). The measured CN were assumed to have a Junge distribution with a "Junge" slope of -3.5 [*Lechner et al.*, 1989].

Input to the current model consisted of median values for O_3, CO, H_2O, and NO (e.g., Figures 3, 6, and 9) as well as median values for NMHCs, temperature, and pressure. Of the potential uncertainties in the model output, that involving the evaluation of appropriate field photolysis rates is perhaps most significant. For example, the J values initially estimated were those based on clear-sky conditions using a two-stream radiative transfer model as discussed by *Crawford et al.* [1996] and as formulated by *Dickerson et al.* [1979]. On the basis of IPCC intercomparison involving 21 different radiative transfer models, the uncertainty in the key photolysis rates $J(O_3) \rightarrow O(^1D)$ and $J(NO_2)$ were estimated to be $\pm$ 9% [*Olson et al.*, 1997]. In this study, J values were further adjusted to simulate actual solar/cloud conditions encountered in the tropical western Pacific using a cloud correction factor (CCF). The CCF was based on the median ratio of $J(NO_2)$ empirically determined on the basis of Eppley radiometer UV measurements [*Madronich*, 1987; *Chameides et al.*, 1990] and $J(NO_2)$ calculated by the two-stream model. As was done in PEM-A, the CCF was also normalized to give a value of unity for clear-sky conditions [*Crawford et al.*, 1996]. For the altitude range of 0-1 km the CCF was estimated to be 0.75, whereas for 1-2 km it was 0.95, and above 2 km the CCF was estimated to be between 0.95 and 1. The assumption made in our final results, therefore, is that the above cited CCFs were, in fact, representative of the tropical-western North Pacific during the time period of sampling.

3.2.2. Photochemical ozone budget. The diurnal average rates for photochemical ozone formation, $F(O_3)$, are given in Table 2. For altitudes below 2 km the difference between the two regimes is seen to be quite small. Above 4 km, however, ozone formation is indicated to be 2 to 6 times larger for the high NO_x regime with the difference increasing with altitude. The closeness of values below 2 km reflects the similarity in chemical conditions for the two regimes and is thus not unexpected. For altitudes above 4 km, the large difference in NO would seem to suggest that the difference in $F(O_3)$ values

Table 2. Diurnal Averaged Rates for O_3 Formation, Destruction, and Tendency

	High NO_x					Low NO_x				
Altitude Range,km	$F(O_3)$, molec/cm³/s	$D(O_3)$, molec/cm³/s	$P(O_3)$, molec/cm³/s	$P(O_3)$, ppbv/d	Median O_3, ppbv	$F(O_3)$, molec/cm³/s	$D(O_3)$, molec/cm³/s	$P(O_3)$, molec/cm³/s	$P(O_3)$, ppbv/d	Median O_3, ppbv
0-1	4.07E+05	8.95E+05	-4.89E+05	-1.77	25.8	3.41E+05	8.86E+05	-5.45E+05	-2.00	18.9
1-2	3.67E+05	9.12E+05	-5.44E+05	-2.23	29.4	3.68E+05	8.47E+05	-4.78E+05	-1.92	19.7
2-4	1.86E+05	2.08E+05	-0.23E+05	-0.11	54.0	2.12E+05	6.65E+05	-4.53E+05	-2.19	21.5
4-6	2.84E+05	2.22E+05	0.62E+05	0.35	50.4	1.26E+05	2.74E+05	-1.48E+05	-0.90	16.9
6-8	2.08E+05	0.75E+05	1.32E+05	0.99	45.3	0.81E+05	1.78E+05	-0.97E+05	-0.69	17.5
8-10	2.10E+05	0.37E+05	1.73E+05	1.62	40.1	0.33E+05	0.26E+05	0.07E+05	0.07	18.9

Read 4.07E+05 as 4.07×10^5

should have been greater. The reason it is not is due to the much higher water vapor levels associated with the low NO_x regime (see Figure 8). Elevated levels of H_2O result in higher predicted peroxy radical concentrations which tend to offset the effects of higher NO mixing ratios associated with the high NO_x regime. Accordingly, the difference in $F(O_3)$ between the two regimes is seen to increase with altitude much slower than might be expected based on the difference in NO levels. Thus these results further demonstrate the important joint role of NO and H_2O in the photochemical formation of ozone [*Chameides et al.*, 1987; *Ridley et al.*, 1992; *Davis et al.*, 1996a].

When evaluated in terms of an integrated column quantity rather than in situ formation, the difference in $F(O_3)$ between the two regimes is seen to be rather modest. As shown in Figure 9, the column-integrated $F(O_3)$ values are 25.5×10^{10} and 16.1×10^{10} molecules/cm²/s for the high and low NO_x regimes, respectively. This means that the column integrated values differ by only a factor of 1.6. Much of this leveling effect reflects the strong influence of large values of $F(O_3)$ at altitudes below 2 km. For example, 30% of the total column integrated O_3 formation for the high NO_x regime and 44% for the low NO_x regime occurs in the lowest 2 km.

In both regimes the reaction of NO with hydroperoxy radicals, (R4), constituted the major formation pathway. Within the BL the contributions from (R4) in the high and low NO_x regimes were 54 and 50%, respectively. Above 2 km the contribution from (R4) gradually increased with altitude, reaching 80% at 8-10 km. By comparison, O_3 formation due to NMHC chemistry, (R6), never exceeded 8%.

The diurnal average rates for photochemical ozone destruction, $D(O_3)$, are also given in Table 2. In this case, the

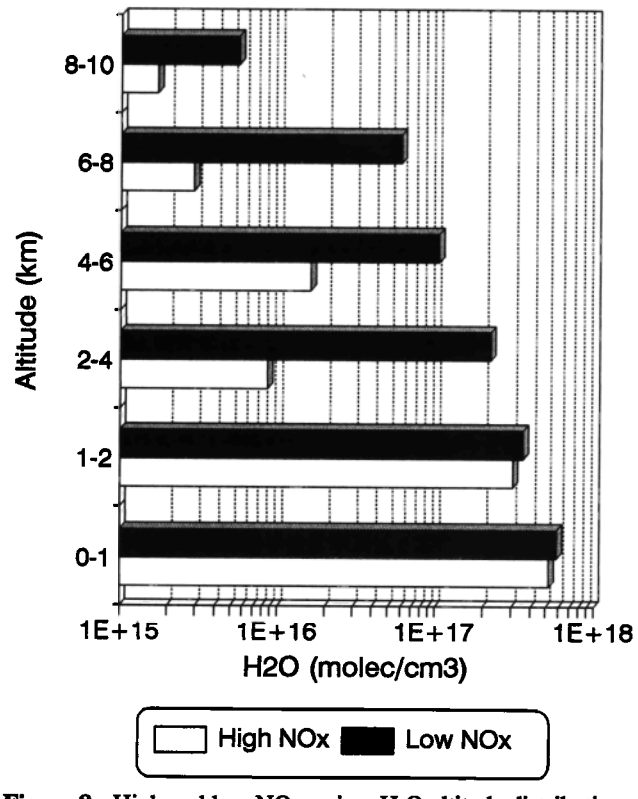

Figure 8. High and low NO_x regime H_2O altitude distributions. Calculated median values were derived from data binned into 1 km increments from 0-2 km and 2 km increments from 2-10 km.

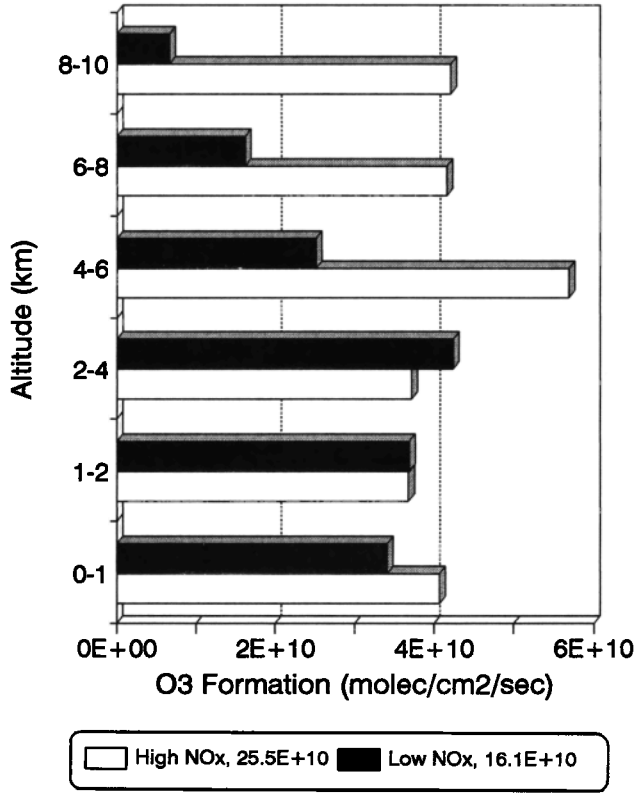

Figure 9. Diurnal-averaged, column integrated values of $F(O_3)$. Values are those calculated from TD box-model runs based on median conditions for high and low NO_x regimes. Net column effects are annotated at the bottom of the figure.

trend in $D(O_3)$ is seen as being completely out of phase with that of formation. When the two regimes differ significantly, it is the low NO_x regime that tends to have the higher $D(O_3)$ value despite having lower ambient O_3 levels. For altitudes below 2 km this difference is seen as being quite small, whereas above this altitude, $D(O_3)$ values for the low NO_x regime are a factor of 2 to 3 times larger than those estimated for the high NO_x regime. This difference in $D(O_3)$ is primarily driven by the large difference in H_2O levels (see Figure 8) with the low NO_x regime having much higher concentrations. This point is further illustrated in the finding that (R3) ($O(^1D) + H_2O$) was the dominant O_3 loss pathway (e.g., 75-80%) for the low NO_x regime at all altitudes. By contrast, for the high NO_x regime, only for BL conditions was (R3) dominant. At altitudes above 2 km, (R3) accounted for only 30% of the loss, while (R7) ($HO_2 + O_3$) defined 52-64% of the total. As mentioned earlier, NO_x levels in the tropics were found to be substantially lower than that required for the destruction of O_3 via (R11) to become significant.

As shown in Figure 10, the column-integrated values for $D(O_3)$ are 28.9×10^{10} and 40.2×10^{10} molecules/cm^2/s for the high and low NO_x regimes, respectively. As discussed for $F(O_3)$, the closeness of the column integrated values of $D(O_3)$ is in large part a reflection of the major influence of $D(O_3)$ in the lowest 2 km. For the high NO_x regime this amounted to 62% of the total column destruction. For the low NO_x regime this value was 43%.

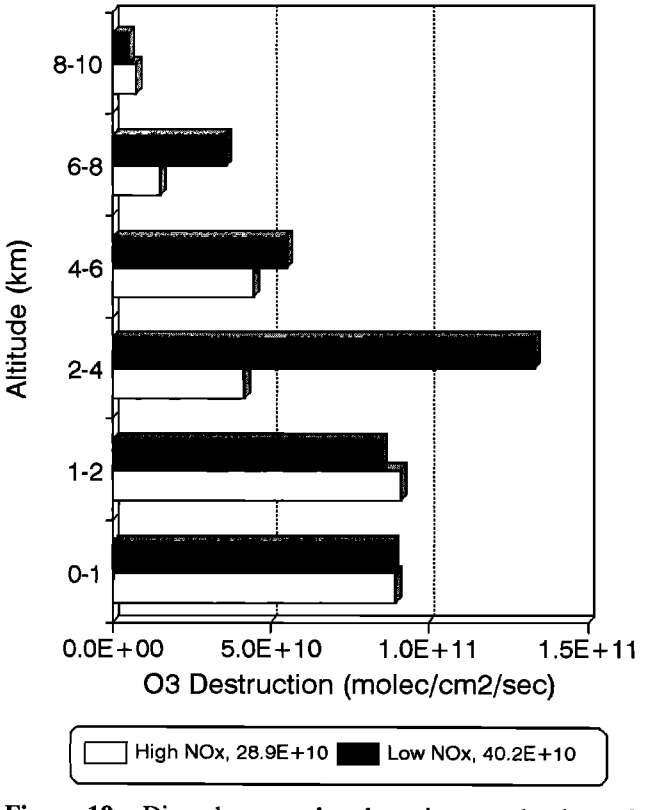

Figure 10. Diurnal-averaged, column-integrated values of $D(O_3)$. Values are those calculated from TD box model runs based on median conditions for high and low NO_x regimes. Net column effects are annotated at the bottom of the figure.

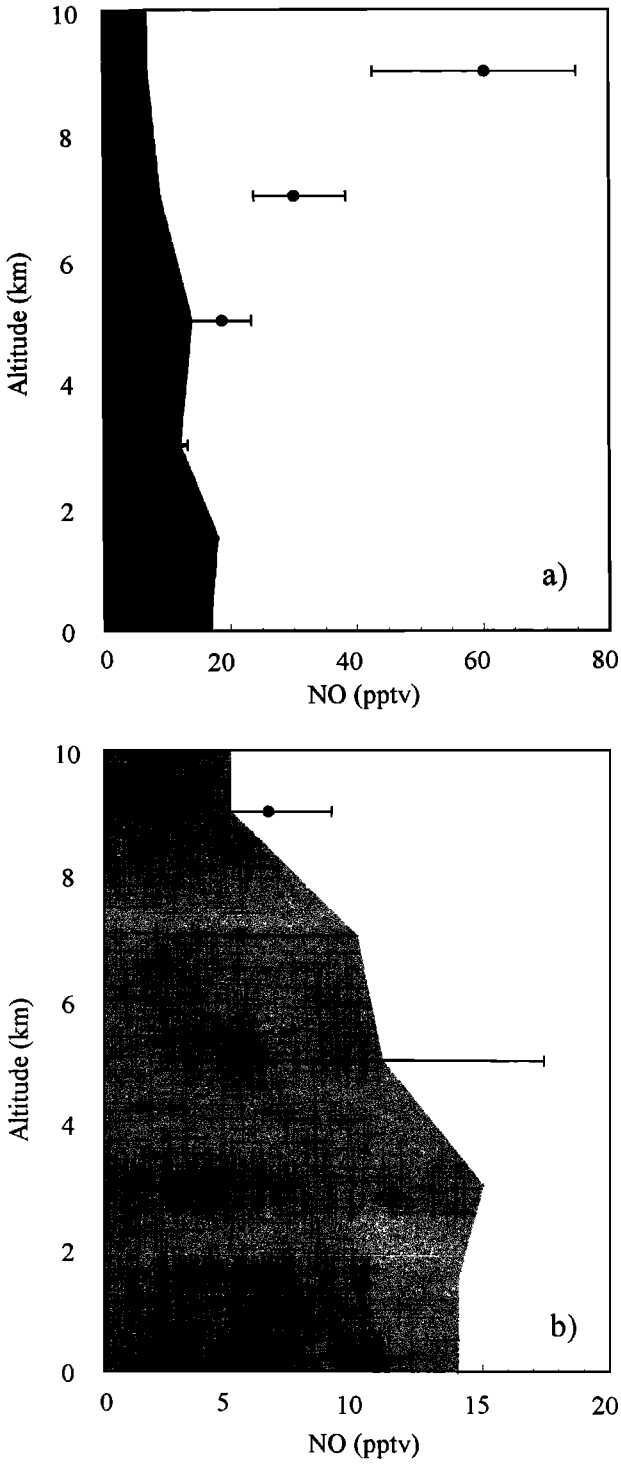

Figure 11. Critical NO (shaded area) and median measured NO (symbols) versus altitude for the (a) high NO_x regime and (b) low NO_x regime. Error bars encompass the inner quartiles.

Although not explicitly shown in equation (2), the possible destruction of O_3 from iodine reactions was also examined. *Davis et al.* [1996b] previously explored this possibility in the case of the tropical PEM-A data. These investigators estimated the iodine chemistry sink to be no larger than 1.8×10^{10} molecules/cm^2/s or approximately 6% of the total O_3 loss. Scaling this estimate to the PEM-B low NO_x regime, with

adjustments for the differences in CH_3I levels, results in an estimated increase in $D(O_3)$ of ~ 4%. This estimate would be shifted still lower for the high NO_x regime since the latter regime had lower CH_3I concentrations.

The net effect of all photochemical processes as related to in situ O_3 levels, $P(O_3)$, has been estimated from equation (3). These results are again provided in Table 2. Quite evident from these is the effect of combining a larger formation rate from the high NO_x regime with a larger destruction rate from the low NO_x regime. In summary, the difference between the two regimes, as expressed in terms of $P(O_3)$ values, becomes greatly amplified. For the high NO_x regime, the impact of $P(O_3)$ on in situ O_3 levels is greatest for the 0-2 km altitude range, reflecting the highest values of $D(O_3)$ and the lowest in situ levels of O_3. The loss of ozone at these altitudes reaches 7% per day. For altitudes in the 2-8 km range, in situ O_3 changes were ±2% or less per day, thus indicating a near photochemical balance. At still higher altitudes (i.e., 8-10 km), O_3 levels are seen increasing at a rate of nearly 4% per day. In sharp contrast the low NO_x regime shows a rather consistent trend of O_3 destruction with in situ O_3 levels in the boundary layer decreasing at the high rate of 10% per day but then gradually falling off with increasing altitude, reaching -4% per day at 6-8 km. Only at 8-10 km is the low NO_x regime observed to be in near photochemical balance. To further illustrate the important role of NO in influencing the trends in $P(O_3)$, we show plotted in Figures 11a and 11b the mixing ratio of this species as a function of altitude and on the same plot have also included the "critical" NO level, i.e., the level of NO

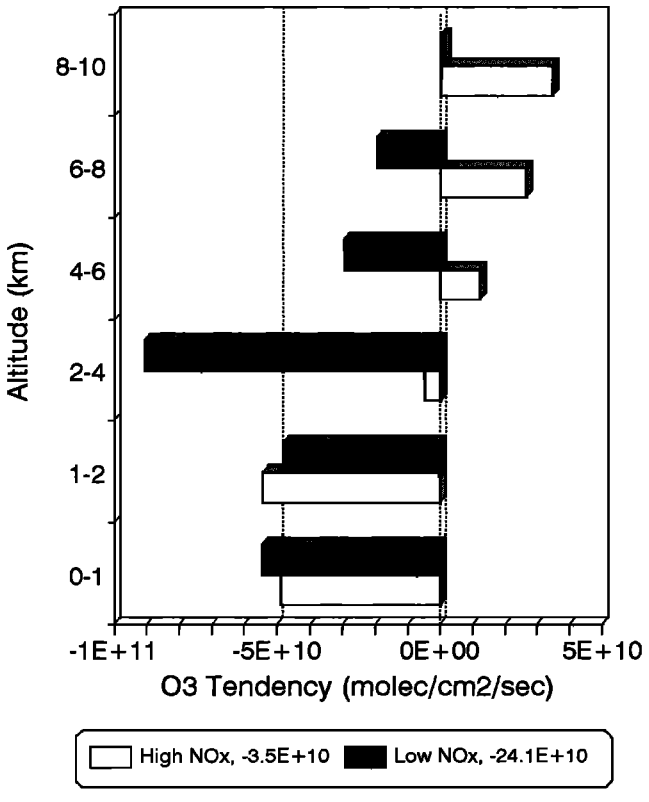

Figure 12. Diurnal-averaged, column integrated values of $P(O_3)$. Values are those calculated from TD box model runs based on median conditions for high and low NO_x regimes. Net column effects are annotated at the bottom of the figure.

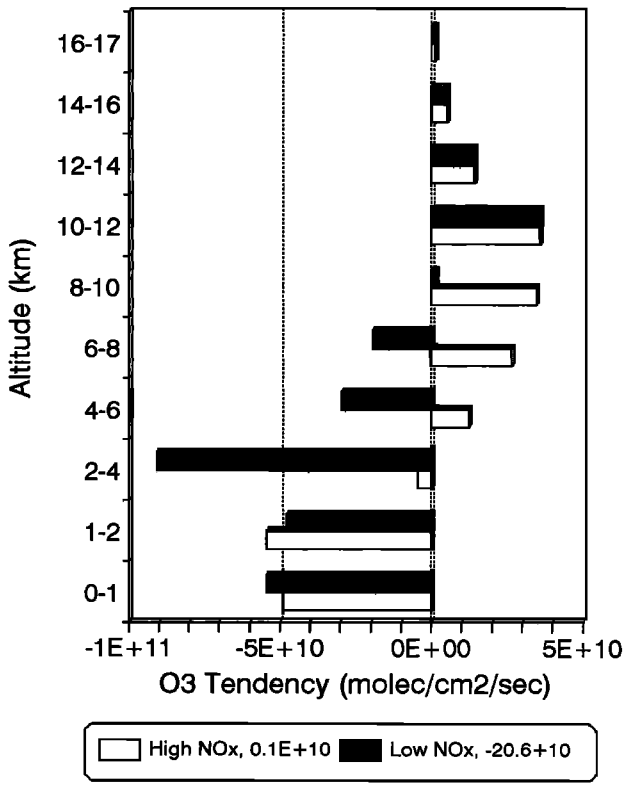

Figure 13. Diurnal-averaged, column integrated values of $P(O_3)$ extrapolated to include the entire tropospheric column, 0-17 km. Results for 0-10 km are those based on TD box-model runs using median conditions for the high and low NO_x regimes. Results for 10-17 km are those estimated assuming 150 pptv of NO. Net column effects are annotated at the bottom of the figure. The addition of 0.5 ppbv of acetone was found to further shift net column effects for the high and low NO_x regimes to 2.9×10^{10} and -17.9×10^{10}, respectively.

at which destruction is balanced by formation. In these figures the solid lines indicate the critical NO, and the symbols show the median measured NO. In this case, both regimes are seen exhibiting a similar trend in critical NO with values starting just above 15 pptv in the BL and then decreasing to less than 10 pptv at 8-10 km. The observations, however, show NO in the high NO_x regime exceeding the critical level by significant amounts above 5 km. By contrast, in the low NO_x regime, NO mixing ratios remain below the critical level until 8-10 km where the two are essentially equal.

In Figure 12, $P(O_3)$ values are shown expressed in terms of column-integrated quantities. From this figure the low NO_x regime is seen as having values that are significantly negative at all altitudes but 8-10 km (i.e., $P(O_3) \approx 0$). This translates into a net ozone column destruction rate of -24×10^{10} molecules/cm^2/s. For comparison purposes, this is a value that is 5 times larger than the O_3 deposition flux to the ocean [*Kawa and Pearson*, 1989; *Lenschow et al.*, 1982]. In contrast to the very negative integrated O_3 picture for low NO_x, the high NO_x regime crosses over to positive values at 4-6 km. Thus the net column effect on O_3, while still destruction, is quite modest, e.g., -3.5×10^{10} molecules/cm^2/s.

When the above values are placed in the context of a percent change per day by folding in the column ozone densities for both regimes (i.e., $2.9x10^{17}$ and $6.5x10^{17}$ molecules/cm^2, low versus high), the previously cited net column $P(O_3)$ values convert to -7.2% and -0.5%/day, respectively. However, this picture of net destruction in all regimes is altered if instead of using 0-10 km as the column height, the full tropopause height of 0-17 km is considered. For example, *Davis et al.* [1996a] found in their analysis of the PEM-A tropical data that ozone formation in the 10-17 km altitude range maximized when NO levels approached approximately 150 pptv. This new limitation reflects the effects on the chemistry from having a limited supply of HO_x. Levels of NO as high as 150 pptv are not inconsistent with the limited observations of NO at altitudes above 10 km during both PEM-A and B.

If for purposes of this analysis we accept the same assumptions as employed by *Davis et al.*, the summary calculations illustrated in Figure 13 indicate that there results a net balance in O_3 formation and destruction for the high NO_x regime (e.g., $0.1x10^{10}$ molecules/cm^2/s) but that there still remains a large net destruction for low NO_x of $-20.6x10^{10}$ molecules/cm^2/s. Further changes were made by including acetone chemistry at levels of 0.5 ppbv [see *Singh et al.*, 1995], as again assumed by *Davis et al.*, but using updated quantum yield data for acetone photolysis that included a dependence on pressure [*A. Ravishankara*, private communication]. Based on this new quantum yield data, estimated photolysis rates at 10 km increased by around a factor of 2. The inclusion of acetone leads to a further positive O_3 shift in each regime of $2.8x10^{10}$ molecules/cm^2/s due to the availability of an additional HO_x source. Thus, after all adjustments are made to the original chemical environment, the low NO_x regime still ends up with an estimated large negative net O_3 column-integrated flux of $-17.9x10^{10}$ molecules/cm^2/s.

On the basis of the seasonally adjusted O_3 column observations reported by *Fishman et al.* [1992], the tropospheric column density for the tropical western Pacific over the seasonal period December-February to March-May should have experienced an increase of as much as 30%. This suggests that the tropospheric O_3 column should have been undergoing a gradual systematic increase. If viewed in this context, the near balance in O_3 formation and destruction, together with the uncertainties associated with $F(O_3)$ in the 10-17 km altitude range, would argue that the O_3 column budget estimated for the high NO_x regime is reasonably consistent with the (TOMS) data analysis of *Fishman et al.* [1992]. It does, however, raise a major question concerning the source of O_3 required to offset the deficit in the low NO_x regime. At these low latitudes it is unlikely that any direct flux from the stratosphere could balance the current estimated deficit of 18-$24x10^{10}$ molecules/cm^2/s. For example, the average strength of the stratosphere-to-troposphere O_3 flux in the northern hemisphere is estimated at only $5x10^{10}$ molecules/cm^2 [*Gidel and Shapiro*, 1980; *Mahlman et al.*, 1980].

Given a similar O_3 budget problem in the analysis of the PEM-A data, *Davis et al.* [1996a] proposed that an alternative to stratospheric O_3 might be the transport of O_3 rich midlatitude tropospheric air into the tropical region. It would seem that a similar argument could also be made for the case of the PEM-B low NO_x regime. For example, during PEM-B the midlatitude sector was a region with average free tropospheric levels of O_3 that were nearly twice those found at comparable altitudes in the low NO_x regime.

Still a second alternative to the transport of stratospheric O_3 into the tropics is the possibility that within the "greater" tropical Pacific basin, O_3 was self-sustaining through photochemistry, thus leading to a balanced budget. Such was the case for the tropical South Atlantic basin investigated during TRACE A [*Jacob et al.*, 1996]; see discussion later in text. During PEM-B, only a brief snapshot of the tropical Pacific was recorded, and this was limited to only the western North Pacific. We may ask, therefore, how representative the low and high NO_x regimes might have been as related to the western Pacific region and also in relationship to the "greater" tropical Pacific. For instance, what might the high NO_x regime have looked like earlier in time? Equally importantly, were there other geographical regions in the tropical Pacific that might have been more favorably influenced by transport of lightning/surface NO_x emissions from the continent (e.g., via Walker circulation)? Quite possibly, NO_x levels in the high NO_x regime, if sampled earlier in time, would have been even higher than those sampled at the time of PEM-B. If so, this regime could have defined a region of significant net O_3 production.

In the absence of observations at other times and at other locations, several model simulations were run to assess the question of how different conditions would have had to be in order to shift a marine area such as our labeled high NO_x regime which was near steady state in O_3 to a significant O_3 source regime. In these simulations an enhancement in NO_x was implemented at altitudes between 4 and 10 km to represent the high altitude outflow of convected air over southeastern Asia into a remote marine environment. Enhancements were increased until the net column production reached a magnitude large enough that it would exceed the possible uncertainties in $F(O_3)$ and $D(O_3)$ (e.g., ~30% of $F(O_3)$ or $10x10^{10}$ molecules/cm^2/s). The results from these runs indicate that the addition of only 30 pptv to median NO_x levels would lead to significant net column production of O_3. Furthermore, time dependent model calculations indicate that it would take just over 1 day between 4-8 km and 2 days at 8-10 km for these enhanced values to decay to the observed median values. Thus the enhancement of 30 pptv would seem to be reasonable based on the isentropic trajectories which suggest that the air parcels sampled in the high NO_x regime were 2-3 days removed from the Pacific Rim.

While the trajectories do not indicate that BL air came from the Pacific Rim, we also explored the possible impact of a 30 pptv enhancement between the BL and the 4 km. In this case, the enhanced NO levels decayed to the observed median values within about 5 hours below 2 km and within 1 day from 2 to 4 km; however, the faster photochemistry at these altitudes resulted in an equivalent impact on the column $F(O_3)$ value. This suggests that an enhancement of only 15 pptv in NO_x at all altitudes would have roughly the same impact on the O_3 column as a 30 pptv enhancement above 4 km. Whether such regimes were actually present in the tropical Pacific at the time of PEM-B is unknown, but clearly, the answer to this question is centrally important to our understanding of the tropical tropospheric O_3 budget.

3.2.3. Comparison with PEM-West A. Although the PEM-A and PEM-B field programs took place in different

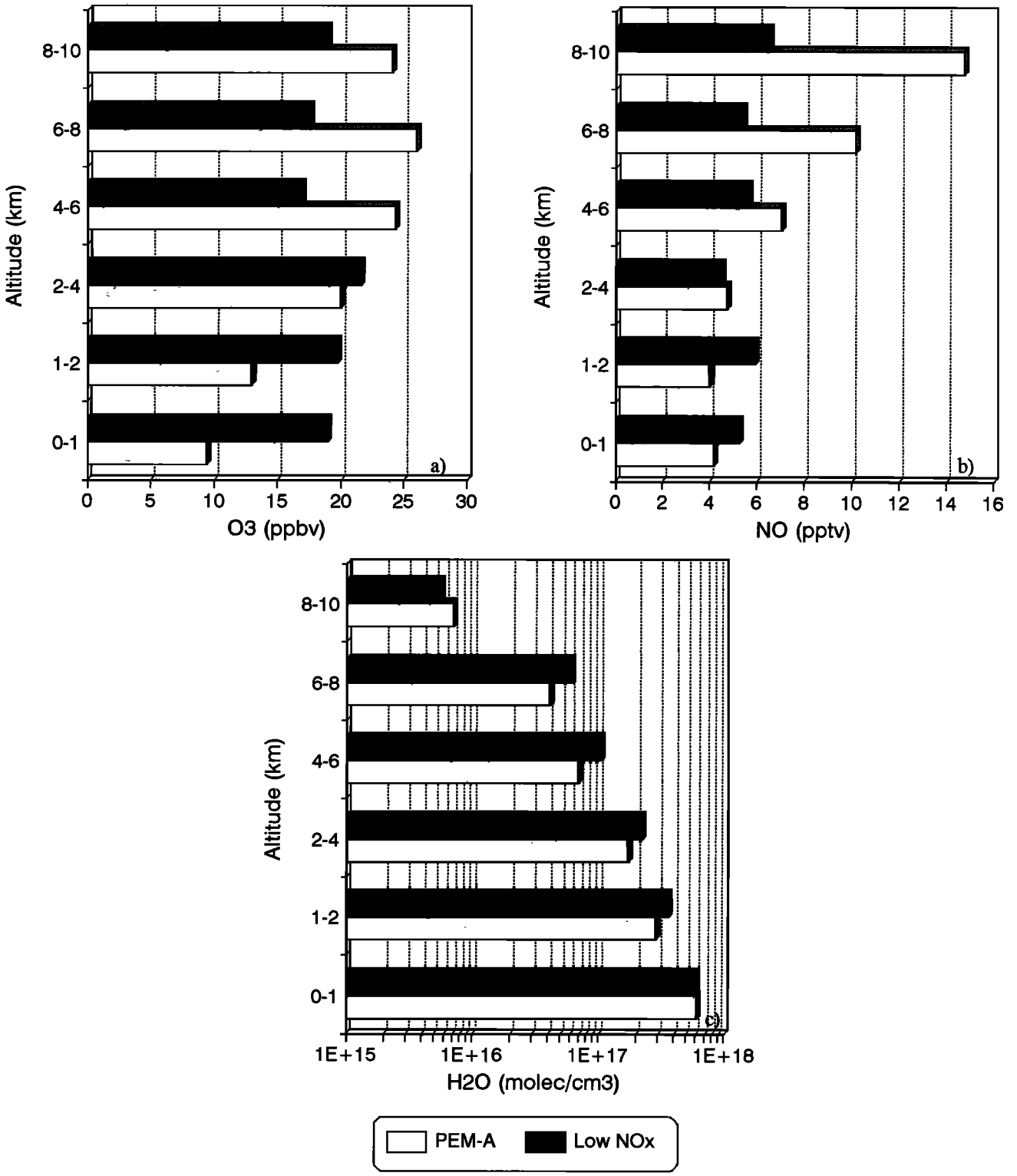

Figure 14. PEM-West A and low NO_x regime altitude distributions for (a) O_3, (b) NO, and (c) H_2O.

seasons, the tropical components of each of these programs appear to share some commonality in terms of their chemical characteristics. For example, on the basis of the analysis of TOMS satellite data for the tropics [*Fishman et al.*, 1992], we estimate that values for the integrated O_3 column should have been similar for both PEM-B (February - March) and PEM-A (September - October). In fact, upon comparing actual in situ O_3 field observations, the column amounts in the PEM-A tropical regime (0-18°N, 120-170°E) were found to compare most favorably (i.e., within 5%) with those observed in the PEM-B low NO_x regime, the latter regime being a factor of 2 lower than that observed for high NO_x. Figure 14a shows the comparison of median O_3 levels for PEM-B low NO_x and PEM-A tropics for the altitude range of 0-10 km. These data

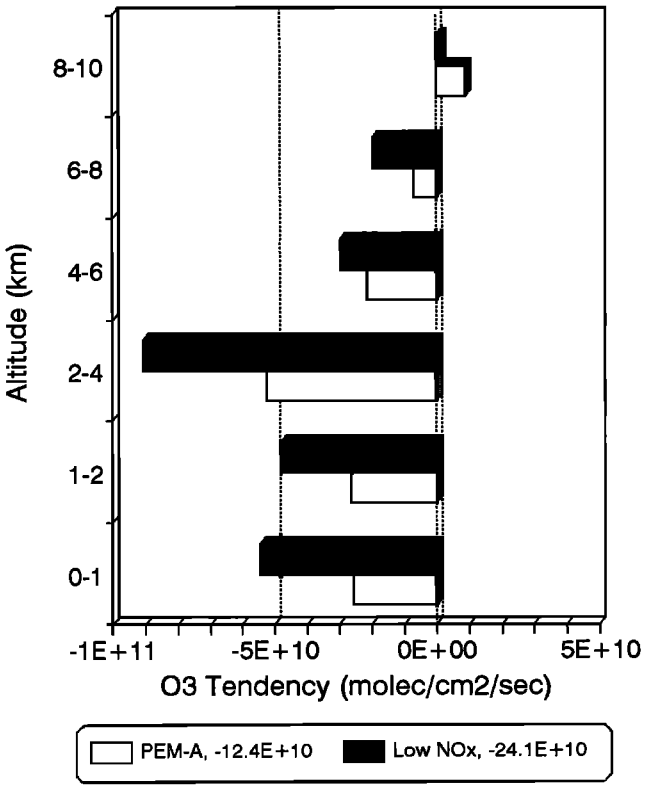

Figure 15. Diurnal-averaged, column integrated values of $P(O_3)$. Values are those calculated from TD box-model runs based on median conditions for PEM-West A and low NO_x regimes. Net column effects are annotated at the bottom of the figure.

indicate that the closeness in O_3 column amounts occurs because excess levels of high altitude O_3 in PEM-A are offset by excess levels of low altitude O_3 in PEM-B low NO_x. (Composite UV DIAL O_3 profiles from PEM-A further support the representativeness of the in situ O_3 data for PEM-A displayed in Figure 14a.)

The PEM-A tropical data also compare more favorably with PEM-B low NO_x for the critical photochemical species NO and H_2O. For instance, Figures 14b and 14c show comparisons of the median values of NO and H_2O. These data indicate that PEM-A NO levels increase gradually with altitude from 5 pptv in the BL to 15 pptv at 8-10 km. This high altitude value falls far below the 60 pptv observed in PEM-B high NO_x but is only 8 pptv greater than that shown for the low NO_x regime. PEM-A H_2O levels are also similar to those recorded for the low NO_x regime, agreeing within a factor of 1.5 at all altitudes.

Despite the cited similarities, the model evaluated photochemical O_3 trends in PEM-A tropical and PEM-B low NO_x were found to be significantly different. These are shown in Figure 15. (Note that the difference in the noontime solar zenith angles for these two data sets was $<4°$). In this case we see that the diurnal-averaged column-integrated $P(O_3)$ values, over the altitude range of 0-10 km, are -12.4×10^{10} molecules/cm^2/s (-3.5%/d) for PEM-A tropics and -24.1×10^{10} molecules/cm^2/s for PEM-B low NO_x. Further analysis revealed that this disparity is largely due to a difference in $D(O_3)$ values. For example, the column-integrated $D(O_3)$ values were -28.4×10^{10} and -40.2×10^{10} molecules/cm^2/s, respectively. By comparison, column integrated $F(O_3)$ values for PEM-A and PEM-B low NO_x were essentially identical, i.e., 16.0×10^{10} and 16.1×10^{10} molecules/cm^2/s.

A key element in understanding the difference between these two data sets lies in the vertical distribution of O_3. As noted above, although O_3 column amounts were found to be almost identical, median O_3 levels differed significantly at some altitudes. In PEM-A, median values increase with altitude from 9 ppbv in the BL to 25 ppbv at 8-10 km. O_3 levels for PEM-B low NO_x remain fairly uniform throughout the troposphere, varying between 17 and 21 ppbv (see Figure 14a). As argued earlier, this uniform O_3 distribution is suggestive of rapid vertical mixing. In this specific case, the photochemical by-product of this mixing is that a larger fraction of the O_3 column gets placed at low altitudes, where in combination with high H_2O levels, O_3 destruction is very high. (Recall that the 0-2 km altitude range dominated the column O_3 destruction in the low NO_x regime, contributing 43% to the total.) These results are quite significant in that they indicate that for two environments having near-identical O_3 column amounts, the vertical distribution of the ozone can have a profound impact on the photochemical O_3 budget. They further suggest that satellite tropospheric O_3 residual maps for tropical marine regions must be interpreted with considerable caution.

While the comparison of PEM-A tropics with PEM-B low NO_x has provided some interesting insights concerning the differences between the two sampling periods, a more quantitative comparison of the regional ozone budget for PEM-A and PEM-B necessarily must include both the low and the high NO_x regimes. As stated earlier, in the absence of any evidence indicating that one of these two regimes was dominant, we have simply assigned equal weight to both and taken the mathematical mean. The result from this averaging gave a value for $P(O_3)$ of -14×10^{10} molecules/cm^2/s for PEM-B which can be compared to PEM-A tropics, as reported by *Davis et al.* [1996a], whose value was -12×10^{10} molecules/cm^2/s. Thus when looked at in terms of the total tropical western Pacific, the net effect on the O_3 budget during each campaign was not significantly different. It is still noteworthy, though, that both column formation and destruction rates in PEM-B exceed those in PEM-A by 30% and 21%, respectively. This is primarily due to the higher NO_x levels at high altitude and higher ozone levels at low altitudes in PEM-B.

3.2.4. Comparison with other high altitude tropical data. Of the other available major tropical data sets (e.g., NASA GTE CITE-1, ABLE-2A/B, and TRACE A), only TRACE A was found to encompass both a comprehensive suite of chemical measurements and a sampling that involved high altitudes. It must be noted, however, that the emphasis of the TRACE program differed from that of PEM-B in that it focused on a region that typically experienced large seasonal influxes of biomass burning emissions (i.e., the South Atlantic basin) [*Thompson et al.*, 1996; *Jacob et al.*, 1996]. Additionally, the TRACE A database encompassed sampling of both continental and marine regions. Despite these differences, both this study and TRACE A have concluded that deep convection in conjunction with transport of NO_x via the Walker circulation were major factors in controlling the tropical ozone budget. A similar hypothesis was put forward earlier by *Davis et al.* [1996a] in their analysis of the PEM-A data.

For the upper free troposphere (i.e., 6-10 km), NO levels observed in TRACE A were somewhat higher than those found

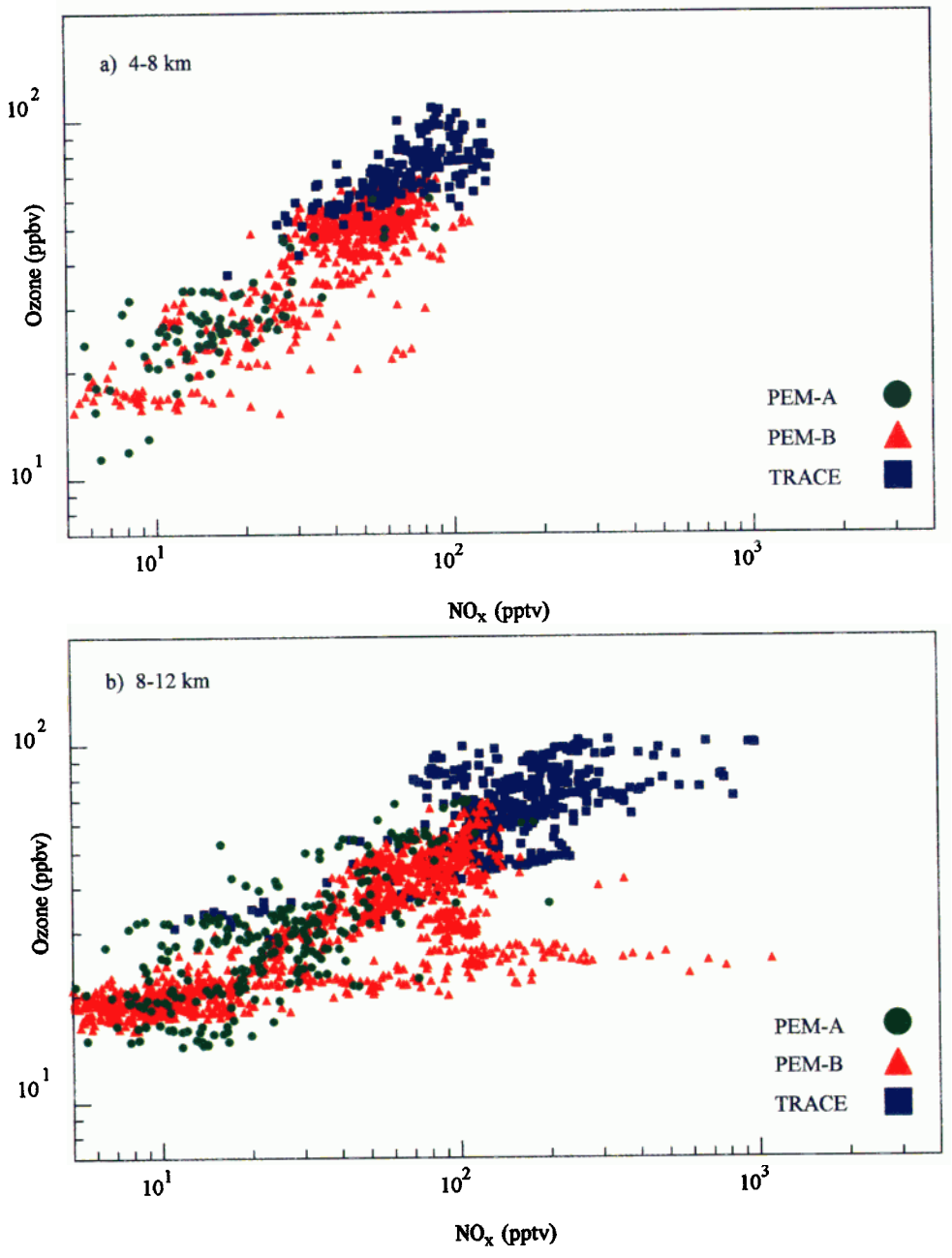

Plate 2. Correlation plot of O_3 versus NO_x for the tropical-marine free troposphere (20°N-20°S): (a) 8-12 km, (b) 4-8 km. Data have been taken from GTE missions PEM-West A (green circles), PEM-West B (red triangles), and TRACE A (blue squares).

for the PEM-B high NO_x regime. This is not unexpected in that additional contributions to the NO_x burden were present due to biomass burning. Ozone levels at these altitudes were also higher by nearly a factor of 1.6, indicating higher net photochemical O_3 production. At lower altitudes, differences in both NO and O_3 were even more pronounced (i.e., factors of 2 or more). Collectively, these differences resulted in column-integrated formation and destruction rates that exceeded PEM-B tropics (high/low NO_x) by factors of 5 and 3, respectively. Not surprisingly, the TRACE A modeling results produced an overall photochemical O_3 picture which involved a balanced budget. Recall that a similar situation was found for the high NO_x PEM-B regime.

To illustrate the major controlling influence of photochemistry on the levels of O_3 in the tropics, Plates 2a and 2b show the relationship between O_3 and NO_x for the tropical-marine free troposphere (e.g., 20°N-20°S, 4-8 and 8-12 km) as observed during GTE missions PEM-West A and B and TRACE A. The trend in these data strongly suggests (e.g., $R^2 = 0.67$, Plate 2a and $R^2 = 0.41$, Plate 2b) that O_3 levels in the tropics at middle and upper free tropospheric altitudes are regulated by photochemistry. The small fraction of data in Plate 2b showing O_3 uncorrelated with increasing levels of NO_x comes from PEM-B flight 6. These data represent a case of significant local injection of NO_x due to lightning-generated NO, the latter being further documented by onboard storm

scope readings and visual sightings. This fresh NO_x had insufficient time to photochemically influence local O_3 levels. Inclusion of these data results in an R^2 value of 0.41, whereas its removal gives an R^2 of 0.57 for the altitude range of 8-12 km. Furthermore, when the 12 TRACE A data points with NO_x levels above 500 pptv are removed, the R^2 value improves to 0.71.

The upper end of these NO_x-O_3 correlations can be understood in terms of air masses which have been influenced by injections of high levels of NO_x into the upper troposphere over continental areas followed by advection out over the tropical Pacific. Such parcels would have high O_3 formation rates; and, given long transport times, would result in significant net production of O_3. By contrast, the lower end of the correlation plot would seem to reflect convection of marine BL air into the upper troposphere. Given the intense destruction of O_3 in the tropical marine BL, such air would necessarily be poor in O_3 and NO_x. As noted already, data from flight 6 depart from the normal trend revealed in Plate 2 in that there were high NO_x levels associated with low O_3. This represents a case where known fresh injections of NO_x from lightning had insufficient time to photochemically produce O_3. Given that most lightning generated NO_x tends to be concentrated near the continents, this represents a less common condition in the tropical marine upper troposphere.

One condition not observed in Plate 2 is high O_3 in the presence of low NO_x. Such air parcels would represent conditions where the NO_x responsible for the buildup of O_3 has been removed via reaction of NO_2 with OH, leaving elevated O_3 behind. That such air parcels are not observed is most likely an indication of the strong role of vertical mixing in the tropical marine troposphere. In addition to bringing low O_3 up from the marine BL, this mixing process also delivers O_3 rich air from the upper troposphere to lower altitudes where higher H_2O levels lead to rapid destruction. This appears to happen with such high frequency that NO_x typically does not have sufficient time to reach its full potential for O_3 production.

This interpretation of the relationship between NO_x-O_3 in the tropics is undoubtedly an oversimplification of the complex interplay between dynamics and photochemistry. It does make the point, however, that any critical assessment of the O_3 budget for the "greater" tropical Pacific will require an examination of the tropical troposphere over both a wide range of altitudes and an expansive range of longitudes. Based on PEM-B results, it is unlikely that such an assessment can be carried out in any simple way using currently available satellite observations of O_3. The strong relationship between NO_x and O_3 also underlines the continuing need for further improvement in our understanding of NO_x sources in the tropics. More than any other factor it is pivotal to our reaching a comprehensive understanding of the tropical O_3 budget.

4. Summary and Conclusions

PEM-B flights in tropical regions of the western Pacific (i.e., 10°S - 20°N) revealed large shifts in observed NO levels as a function of geographical location. This shift was most pronounced over the altitude range 8-10 km where the median NO level for flights 5-8 was found to exceed that from flights 9 and 10 by 1 order of magnitude (i.e., 60 versus 6 pptv). The geographical regions encompassing these two flight groupings define what have been labeled "high" and "low" NO_x regimes.

Isentropic back trajectories indicate a clear difference in the source regions for these two regimes. Air parcels from the low NO_x regime appear to track back to the remote South Pacific, whereas the high NO_x regime involves parcels that originated in the northern hemisphere and that tend to track back to the Asian continent. Further differences were found when comparing chemical tracers in each regime. The low NO_x regime saw enhancements in CH_3I and DMS in conjunction with depressed but uniformly mixed O_3 levels. These observations are seen as being most consistent with marine convection. Thus it is not surprising that this region also revealed little evidence of lightning-generated NO_x. In sharp contrast the high NO_x regime showed significant enhancements in C_3H_8, ^{210}Pb, and organic acids such as $CH_3C(O)OH$. These observations are more consistent with air parcels having experienced deep convection over a continental landmass. The observed high altitude levels of C_3H_8, when ratioed against estimated values of NO_x, tend to argue that the major source of NO_x in this regime was lightning, not transport of surface emissions. This conclusion was also found to be consistent with DMSP satellite observations recorded during the PEM-B sampling period. Even so, we cannot at this time rule out the possibility that much of the NO_x was being generated by the efficient recycling of unidentified NO_y species through yet unknown/nondocumented mechanisms.

Time-dependent photochemical box-model simulations revealed large differences between the two regimes as related to their respective photochemical O_3 budgets. These differences mainly could be attributed to the large differences between the two regimes in the levels of NO and H_2O. For free tropospheric altitudes, in situ O_3 formation in the high NO_x regime exceeded that for low NO_x by factors of 2-6. By contrast, in situ O_3 destruction for the low NO_x regime exceeded that estimated for the high NO_x regime by as much as a factor of 3. The latter difference was primarily driven by high H_2O levels associated with the low NO_x regime.

The column integrated values of $F(O_3)$ and $D(O_3)$ were found to be dominated by photochemical activity in the lowest 2 km. For this altitude range both regimes had somewhat similar conditions; thus, differences in the column integrated values were smaller than what might have been expected. Even so, the higher value for $F(O_3)$ for the high NO_x regime, in combination with a lower value for $D(O_3)$, resulted in an amplification of the overall photochemical effect. Thus estimates of $P(O_3)$ indicate that the low NO_x regime was one of strong destruction (i.e., -24×10^{10} molecules/cm^2/s or -7.2%/d), whereas high NO_x showed only weak destruction (i.e., -3.5×10^{10} molecules/cm^2/s or -0.5%/d) when evaluated over an altitude range of 0-10 km. When evaluated for a 0-17 km tropopause height with added acetone chemistry, the high NO_x regime switched signs and became a small net O_3 producer (2.9×10^{10} molecules/cm^2/s). The low NO_x regime, on the other hand, remained strongly destructive, but the rate dropped to -17.9×10^{10} molecules/cm^2/s.

The large rate of O_3 destruction in the low NO_x regime was found to be inconsistent with seasonally averaged tropospheric TOMS data, which suggest that tropical O_3 levels should either have been at steady state or have been increasing with the onset of the spring season. Two basic mechanisms were proposed to reconcile this situation. The first involved the transport of O_3 rich midlatitude air into the tropics from midlatitudes. Analysis of the PEM-B midlatitude data base has revealed that this

region was both O_3 and NO_x rich. The second mechanism allowed for the existence of still other high NO_x regimes in the "greater" tropical Pacific as well as other low NO_x regions. It was proposed that this ensemble of regimes might lead to near-self-sustaining levels of column O_3 in the tropics. Thus in the latter scenario O_3 would be predominantly controlled by photochemistry. Obviously, combinations of mechanisms 1 and 2 would also be possible.

Expanding on the earlier hypothesis by *Davis et al.* [1996a], the existence of Pacific high NO_x regimes as well as possibly "super" NO_x regimes (i.e., regimes showing significant positive $P(O_3)$ values) are viewed here as regions uniquely modified by transport processes. They are regions that most likely experienced the effects of long-range transport (e.g., Walker circulation) of air parcels that originated over a landmass that had experienced significant deep convection. The photochemical effects from these parcels can be most clearly seen at high altitudes, but they also become evident in those regions where sinking motion brings these NO_x- energized parcels (i.e., due to lightning and/or surface NO_x emissions) down to lower altitudes. This process in combination with the countereffects resulting from deep marine convection along the ITCZ now appear to be the major components impacting on the photochemical O_3 budget of the tropical Pacific. However, the database from which this expanded hypothesis is based is still far too limited, and new observations at different geographical locations and times of year are needed.

Evidence supporting the notion that photochemistry in the tropics routinely has a major impact on the levels of O_3 was demonstrated in our finding a strong correlation between O_3 and NO_x levels at free tropospheric altitudes for the Pacific field programs PEM-A and PEM-B and also for the South Atlantic study TRACE A. In addition, these observations again point to the long-standing critical need of a comprehensive understanding of both primary and secondary sources of NO_x for purposes of understanding the tropical O_3 budget.

Acknowledgements. This work was supported in part by funds from the National Aeronautics and Space Administration under grants NCC-1-148 and 1438 and by the Atmospheric Chemistry Project of the Climate and Global Change Program of the National Oceanic and Atmospheric Administration. D. D. Davis would also like to thank the project office at NASA Langley Research Center and the flight crews at NASA Ames Research Center for their dedicated support of the PEM-West B program. He would also like to acknowledge the efforts of Steven Goodman of the NASA George C. Marshall Space Flight Center, and Ross Swick, Greg Scharfen, Rob Bauer and Kenny Knowles of the National Snow and Ice Data Center, CIRES, University of Colorado, in producing the lightning database.

References

Beck, J. P., C. E. Reeves, F. A. A. M. de Leeuw, and S. A. Penkett, The effect of aircraft emissions on tropospheric ozone in the northern hemisphere, *Atmos. Environ.*, *26A*, 17-29, 1992.

Borucki, W. J. and W. L. Chameides, Lightning: Estimates of the rates of energy dissipation and nitrogen fixation, *Rev. Geophys.*, *22*, 363-372, 1984.

Chameides, W. L., and J. C. G. Walker, A photochemical theory of tropospheric ozone, *J. Geophys. Res.*, *78*, 8751-8760, 1973.

Chameides, W. L., and D. D. Davis, Iodine: Its possible role in tropospheric photochemistry, *J. Geophys. Res.*, *85*, 7383-7398, 1980.

Chameides, W. L., D. D. Davis, M. O. Rodgers, J. Bradshaw, S. Sandholm, G. Sachse, G. Hill, G. Gregory, and R. Rasmussen, Net ozone photochemical production over the eastern and central North Pacific as inferred from GTE/CITE 1 observations during fall 1983, *J. Geophys. Res.*, *92*, 2131-2152, 1987.

Chameides W. L., et al., Observed and model-calculated NO_2/NO ratios in tropospheric air sampled during the NASA GTE/CITE 2 field study, *J. Geophys. Res.*, *95*, 10,235-10,247, 1990.

Chatfield, R. B., Anomalous HNO_3/NO_x ratio of remote tropospheric air: Conversion of nitric acid to formic acid and NO_x?, *Geophys. Res. Lett.*, *21*, 2705-2708, 1994.

Chatfield, R., and A. Delany, Convection links biomass burning to increased tropical ozone: However, models will tend to over predict O_3, *J. Geophys. Res.*, *95*, 18,473-18,488, 1990.

Chen, T.-Y., Three-dimensional distribution of nonmethane hydrocarbons and halocarbons over the northwestern Pacific during the 1991 Pacific Exploratory Mission (PEM-West A) and the temporal and spatial variation of oceanic CH_3I emissions, Graduate thesis, Univ. of Calif., Irvine, 1996.

Clarke, A. D., Atmospheric nuclei in the Pacific midtroposphere: Their nature, concentration and evolution, *J. Geophys. Res.*, *98*, 20,633-20,647, 1993.

Crawford, J., et al., Photostationary state analysis of the NO_2-NO system based on airborne observations from the western and central North Pacific, *J. Geophys. Res.*, *101*, 2053-2072, 1996.

Crutzen, P., A discussion of the chemistry of some minor constituents in the stratosphere and troposphere, *Pure Appl. Geophys.*, *106-108*, 1385-1399, 1973.

Davis, D. D., J. D. Bradshaw, M. O. Rodgers, S. T. Sandholm, and S. KeSheng, Free tropospheric and boundary layer measurements of NO over the central and eastern North Pacific Ocean, *J. Geophys. Res.*, *92*, 2049-2070, 1987.

Davis, D. D., et al., Assessment of the ozone photochemistry tendency in the western North Pacific as inferred from PEM-West A observations during the fall of 1991, *J. Geophys. Res.*, *101*, 2111-2134, 1996a.

Davis, D., J. Crawford, S. Liu, S. McKeen, A. Bandy, D. Thornton, F. Rowland, and D. Blake, Potential impact of iodine on tropospheric levels of ozone and other critical oxidants, *J. Geophys. Res.*, *101*, 2135-2147, 1996b.

Dentener F. J., and P. J. Crutzen, Reaction of N_2O_5 on tropospheric aerosols: Impact on the global distributions of NO_x, O_3, and OH, *J. Geophys. Res.*, *98*, 7149-7163, 1993.

Dibb, J. E., R. W. Talbot, B. L. Lefer, E. Scheuer, G. L. Gregory, E. V. Browell, J. D. Bradshaw, S. T. Sandholm, and H. B. Singh, Distributions of beryllium 7 and lead 210, and soluble aerosol-associated ionic species over the western Pacific: PEM-B, February-March 1994, *J. Geophys. Res.* this issue.

Dickerson, R. R., D. D. Stedman, W. L. Chameides, P. J. Crutzen, and J. Fishman, Actinometric measurements and theoretical calculations of $J(O_3)$, the rate of photolysis of ozone to $O(^1D)$, *Geophys. Res. Lett.*, *6*, 833-837, 1979.

Drummond, J. W., D. H. Ehhalt, and A. Volz, Measurements of nitric oxide between 0 and 12 km altitude and 67°N-60°S latitude obtained during STRATOZ III, *J. Geophys. Res.*, *93*, 15,831-15,849, 1988.

Ehhalt, D. H., and J. W. Drummond, The tropospheric cycle of NO_x, in *Chemistry of the Unpolluted and Polluted Troposphere*, edited by H. W. Georgii and W. Jaeschke, pp. 219-251, D. Reidel, Norwell, Mass., 1982.

Ehhalt, D. H., F. Rohrer, and A. Wahner, Sources and distribution of NO_x in the upper troposphere at northern midlatitudes, *J. Geophys. Res.*, *97*, 3725-3738, 1992.

Fan, S.-M., D. J. Jacob, D. L. Mauzerall, J. D. Bradshaw, S. T. Sandholm, D. R. Blake, R. W. Talbot, G. L. Gregory, and G. W. Sachse, Origin of tropospheric NO_x over subarctic eastern Canada in summer, *J. Geophys. Res.*, *99*, 16,867-16,877, 1994.

Fehsenfeld, F., and S. Liu, Tropospheric ozone: Distribution and sources, in *Global Atmospheric Chemical Change*, edited by C. Hewitt and W. Sturges, pp. 169-231, Elsevier Sci, New York, 1993.

Fishman, J., S. Solomon, and P. J. Crutzen, Observational and theoretical evidence in support of a significant in situ photochemical source of tropospheric ozone, *Tellus, 31*, 432-446, 1979.

Fishman, J., V. G. Brackett, and K. Fakhruzzaman, Distribution of tropospheric ozone in the tropics from satellite and ozonesonde measurements, *J. Atmos. Terr. Phys., 54*, 589-597, 1992.

Fishman, J., J. M. Hoell Jr., R. D. Bendura, R. J. McNeal, and V. W. J. H. Kirchoff, NASA GTE TRACE A Experiment (September-October 1992): Overview, *J. Geophys. Res., 101*, 23,865-23,880, 1996.

Folkins, I. A., et al., O_3, NO_y, and NO_x/NO_y in the upper troposphere of the equatorial Pacific, *J. Geophys. Res., 100*, 20,913-20,926, 1995.

Gidel, L. T., and M. A. Shapiro, General circulation model estimates of the net vertical flux of ozone in the lower stratosphere and the implications for the tropospheric ozone budget, *J. Geophys. Res., 85*, 4049-4058, 1980.

Goodman, S. J., and H. J. Christian, Global observations of lightning, in *Atlas of Satellite Observations Related to Global Change*, edited by R. J. Gurney, J. L. Foster, and C. L. Parkinson, pp. 191-219, Cambridge Univ. Press, New York, 1993.

Gregory, G., J. Hoell, Jr., A. Torres, M. A. Carroll, B. R. Ridley, M. Rodgers, J. Bradshaw, S. Sandholm, and D. Davis, An intercomparison of airborne nitric oxide measurements: A second opportunity, *J. Geophys. Res., 95*, 10,129-10,138, 1990.

Hameed, S., O. G. Paidoussis, and R. W. Stewart, Implications of natural sources for the latitude gradient of NO_y in the unpolluted troposphere, *Geophys. Res. Lett., 8*, 591-594, 1981.

Harriss, R. C., et al., The Amazon Boundary Layer Experiment (ABLE 2A): Dry season 1985, *J. Geophys. Res., 93*, 1351-1360, 1988.

Harriss, R. C., et al., The Amazon Boundary Layer Experiment: Wet season 1987, *J. Geophys. Res., 95*, 16,721-16,736, 1990.

Harriss, R. C., et al., The Arctic Boundary Layer Expedition (ABLE 3A): July-August 1988, *J. Geophys. Res., 97*, 16,383-16,394, 1992.

Harriss, R. C., et al., The Arctic Boundary Layer Expedition (ABLE 3B): July-August 1990, *J. Geophys. Res., 99*, 1635-1643, 1994.

Hoell, J. M., Jr., G. L. Gregory, D. S. McDougal, M. A. Carroll, M. McFarland, B. A. Ridley, D. D. Davis, J. Bradshaw, M. O. Rodgers, and A. L. Torres, An intercomparison of nitric oxide measurement techniques, *J. Geophys. Res., 90*, 12,843-12,851, 1985.

Hoell, J. M., Jr., G. L. Gregory, D. S. McDougal, A. L. Torres, D. D. Davis, J. Bradshaw, M. O. Rodgers, B. A. Ridley, and M. A. Carroll, Airborne intercomparison of nitric oxide measurement techniques, *J. Geophys. Res., 92*, 1995-2008, 1987.

Hoell, J. M., D. D. Davis, S. C. Liu, R. Newell, M. Shipham, H. Akimoto, R. J. McNeal, R. J. Bendura, and J. W. Drewry, Pacific Exploratory Mission-West (PEM-West A): September-October 1991, *J. Geophys. Res., 101*, 1641-1653, 1996.

Hoell, J. M., et al., Pacific Exploratory Mission-West (Phase B): February-March 1994, *J. Geophys. Res.*, this issue.

Jacob, D., et al., Summertime photochemistry of the troposphere at high northern latitudes, *J. Geophys. Res., 97*, 16,421-16,431, 1992.

Jacob, D. J., et al., Origin of ozone and NO_x in the tropical troposphere: A photochemical analysis of aircraft observations over the South Atlantic basin, *J. Geophys. Res., 101*, 24,235-24,250, 1996.

Jeffries, H. E., Photochemical air pollution, in *Composition, Chemistry, and Climate of the Atmosphere*, edited by H. B. Singh, pp. 308-348, Van Nostrand Reinhold, New York, 1995.

Kasibhatla, P. S., H. Levy II, W. J. Moxim, and W. L. Chameides, The relative impact of stratospheric photochemical production on tropospheric NO_y levels, *J. Geophys. Res., 96*, 18,631-18,646, 1991.

Kasibhatla, P. S., H. Levy II, and W. J. Moxim, Global NO_x, HNO_3, PAN, and NO_y distributions from fossil fuel combustion emissions: A model study, *J. Geophys. Res., 98*, 7165-7180, 1993.

Kawa, S. R., and R. Pearson Jr., Ozone budgets from the dynamics and chemistry of marine stratocumulus experiment, *J. Geophys. Res., 94*, 9809-9817, 1989.

Kley, D., P. J. Crutzen, H. G. J. Smit, H. Vomel, S. J. Oltmans, H. Grassl, and V. Ramanathan, Observations of near-zero ozone concentrations over the convective Pacific: Effects on air chemistry, *Science, 274*, 230-233, 1996.

Kumar, P. P., G. K. Manohar, and S. S. Kandalgaonkar, Global distribution of nitric oxide produced by lightning and its seasonal variation, *J. Geophys. Res., 100*, 11,203-11,208, 1995.

Lechner, I. S., G. W. Fisher, H. R. Larsen, M. J. Harvey, and R. A. Knobben, Aerosol size distributions in the southwest Pacific, *J. Geophys. Res., 94*, 14,893-14,903, 1989.

Lenschow, D. H., R. Pearson Jr., and B. B. Stankor, Measurements of ozone vertical flux to ocean and forest, *J. Geophys. Res., 87*, 8833-8837, 1982.

Levy H., II, and W. J. Moxim, Simulated global distribution and deposition of reactive nitrogen emitted by fossil fuel combustion, *Tellus, 41*, 256-271, 1989.

Levy H., II, W. J. Moxim, and P. S. Kasibhatla, A global 3-dimensional time-dependent lightning source of tropospheric NO_x, *J. Geophys. Res., 101*, 22,911-22,922, 1996.

Liu S. C., Possible effects on tropospheric O_3 and OH due to NO emissions, *Geophys. Res. Lett., 4*, 325-328, 1977.

Liu, S. C., D. Kley, M. McFarland, J. D. Mahlman, and H. Levy II, On the origin of tropospheric ozone, *J. Geophys. Res., 85*, 7546-7552, 1980.

Liu, S. C., M. Trainer, F. C. Fehsenfeld, D. D. Parrish, E. J. Williams, D. W. Fahey, G. Hubler, and P. C. Murphy, Ozone production in the rural troposphere and the implications for regional and global ozone distributions, *J. Geophys. Res., 92*, 4191-4207, 1987.

Logan, J. A., Nitrogen oxides in the troposphere: Global and regional budgets, *J. Geophys. Res., 88*, 10,785-10,807, 1983.

Madronich, S., Intercomparison of NO_2 photodissociation and U.V. radiometer measurements, *Atmos. Environ., 21*, 569-578, 1987.

Mahlman, J. D., H. Levy II, and W. J. Moxim, Three-dimensional tracer structure and behavior as simulated in two ozone precursor experiments, *J. Atmos. Sci., 37*, 655-685, 1980.

McFarland, M., D. Kley, J. W. Drummond, A. L. Schmeltekopf, and R. H. Winkler, Nitric oxide measurements in the equatorial Pacific region, *Geophys. Res. Lett., 6*, 605-608, 1979.

Olson, J., et al., Results from the IPCC photochemical model intercomparison (PhotoComp), *J. Geophys. Res., 102*, 5979-5991, 1997.

Orville, R. E., and R. W. Henderson, Global distribution of midnight lightning: September 1977 to August 1978, *Mon. Weather Rev., 114*, 2640-2653, 1986.

Penner, J. E., C. S. Atherton, J. Dignon, S. J. Ghan, J. J. Walton, and S. Hameed, Tropospheric nitrogen: A three-dimensional study of sources, distributions, and deposition, *J. Geophys. Res., 96*, 959-990, 1991.

Ridley, B. A., S. Madronich, R. B. Chatfield, J. G. Walega, R. E. Shetter, M. A. Carroll, and D. D. Montzka, Measurements and model simulations of the photostationary state ratio during the Mauna Loa Observatory Photochemical Experiment: Implications for radical concentrations and ozone production and loss rates, *J. Geophys. Res., 97*, 10,375-10,388, 1992.

Singh, H. B., D. O'Hara, D. Herlth, J. D. Bradshaw, S. T. Sandholm, G. L. Gregory, G. W. Sachse, D. R. Blake, P. J. Crutzen, and M. A. Kanakidou, Atmospheric measurements of peroxyacetyl nitrate and other organic nitrates at high latitudes: Possible sources and sinks, *J. Geophys. Res., 97*, 16,511-16,522. 1992.

Singh, H. B., M. Kanakidou, P. J. Crutzen, and D. J. Jacob, High concentrations and photochemical fate of oxygenated

hydrocarbons in the global troposphere, *Nature*, *378*, 50-54, 1995.

Smyth, S., et al., Factors influencing the upper free tropospheric distribution of reactive nitrogen over the South Atlantic during the TRACE A experiment, *J. Geophys. Res.*, *101*, 24,165-24,186, 1996.

Solomon, S., R. R. Garcia, and A. R. Ravishankara, On the role of iodine in ozone depletion, *J. Geophys. Res.*, *99*, 20,491-20,499, 1995.

Talbot, R. W., et al., Chemical characteristics of continental outflow from Asia to the troposphere over the western Pacific Ocean during February-March 1994: Results from PEM-West B, *J. Geophys. Res.*, this issue.

Thompson, A. M., et al., Ozone observations and a model of marine boundary layer photochemistry during SAGA 3, *J. Geophys. Res.*, *98*, 16,955-16,968, 1993.

Thompson, A. M., et. al., Where did tropospheric ozone over southern Africa and the tropical Atlantic come from in October 1992? Insights from TOMS, GTE/TRACE A, and SAFARI 1992, *J. Geophys. Res.*, *101*, 24,251-24,278, 1996.

Thornton, D. C., A. R. Bandy, B. W. Blomquist, D. D. Davis, and R. W. Talbot, Sulfur dioxide as a source of condensation nuclei in the upper troposphere of the Pacific Ocean, *J. Geophys. Res.*, *101*, 1883-1890, 1996.

Turman, B. N., and B. C. Edgar, Global lightning distributions at dawn and dusk, *J. Geophys. Res.*, *87*, 1191-1206, 1982.

Wuebbles, D. J., D. Maiden, R. K. Seals Jr., S. L. Baughcum, M. Metwally, and A. Mortlock, Emissions scenarios development: Report of the emissions scenarios committee, in *The Atmospheric Effects of Stratospheric Aircraft: A Third Program Report*, edited by R. S. Stolarski and H. L. Wesoky, 1993.

B. Anderson, E. Browell, J. Barrick, J.H. Crawford, G. Gregory, and G. Sachse, NASA Langley Research Center, Hampton, VA.. (e-mail: b.e.anderson@larc.nasa.gov; e.v.browell@larc.nasa.gov; j.d.barrick@larc.nasa.gov; crawford@asdsun.larc.nasa.gov; g.l.gregory@larc.nasa.gov; g.w.sachse@larc.nasa.gov)

D. Blake, Department of Chemistry, CMOO-Gen Dept., CM-30, University of California-Irvine, Irvine, CA, 92717. (e-mail: dblake@orion.oac.uci.edu)

G. Chen, D.D. Davis, S. Sandholm, and S. Liu, School of Earth and Atmospheric Sciences, Georgia Institute of Technology, 221 Bobby Dodd Way, Atlanta, GA 30332. (e-mail: gc37@prism.gatech.edu; douglas.davis@eas.gatech.edu; scott.sandholm@eas.gatech.edu; shaw.liu@eas.gatech.edu)

Y. Kondo, Solar Terrestrial Environ. Lab., Nagoya University, Toyokawa, Aichi, 442, Japan. (email: kondo@stelab.nagoya.u.ac.jp)

J. Merrill, Graduate School of Oceanography, Univ. of Rhode Island, Narragansett, RI 02882. (email: jmerrill@boreas.gso.uri.edu)

R. Pueschel, NASA Ames Research Center, M.S. 245-4 /Bldg. 245, Rm 142, Moffett Field, CA94035. (e-mail: rudolf_pueschel@qmgate.arc.nasa.gov)

R. Talbot, Institute for the Study of Earth, Oceans, and Space, Mores Hall, University of New Hampshire, Durham, NH 03824, (e-mail: rwt@christa.unh.edu)

(Received March 8, 1996; revised December 31, 1996; accepted December 31, 1996.)